Selective and Non-selective Synthesis of Carbon Nanotubes (CNTs) by Chemical Vapor Deposition (CVD) Characterization: Catalysts and Underlayers Effects on Field Emission Properties

by

Chung-Nan Tsai

A thesis submitted to the Graduate Faculty of
Auburn University
in partial fulfillment of the
requirements for the Degree of
Master of Science

Auburn, Alabama
Dec 08, 2012

Keywords: Carbon Nanotube, Chemical Vapor Deposition, Field Emission

Approved by

Hulya Kirkici, Chair, Professor of Electrical and Computer Engineering
Guofu Niu, Professor of Electrical and Computer Engineering
Michael Baginski, Associate Professor of Electrical and Computer Engineering

Abstract

Since the discovery of carbon nanotubes (CNTs), they have been attracted much attention with abundant potential applications based on their outstanding properties. CNTs are well-known for their superior mechanical strength and low weight, excellent heat conductance, and varying electronic properties depending on their helicity and diameter. In particular, the recent research studies have reported that CNTs have excellent electrical field emission properties, with high emission currents at low electric field strength due to the high aspect ratio (small diameter and relatively long length). As a result, CNTs are considered as one of the promising materials as cold-cathode field emission sources, especially for application requiring high-current densities and lightweight packaging.

In this research work, the selective and non-selective multi-wall CNTs (MWCNTs) are grown by using chemical vapor deposition (CVD) technique. Then, their field emission properties are examined in a high pressure vacuum chamber of around 10^{-7} to 10^{-6} Torr. MWCNTs are grown onto various underlying layers such as SiO_2,Ti ,and W-coated silicon substrates. Thermal CVD furnace containing gas mixtures of acetylene and argon is used to grow CNTs. The growth conditions such as catalyst types and thickness, gas flow rate and deposition temperature are discussed. Effects of different catalysts with various underlayers on the field emission properties of CNTs are studied and results are presented. The measurement results indicate that CNTs have significant field emission capabilities to be used as cold cathode materials.

Acknowledgments

First of all, with a deep sense of gratitude, I wish to thank my thesis advisor, Prof. Hulya Kirkici, for her guidance throught my research work, for her encougement of my professional development, and for her advise on organizing and writing this thesis. I am also very grateful to Prof. Guofu Niu and Prof. Michael Baginski for their time to review my thesis.

During the period of my M.S. study in Auburn, I would like to thank Dr. Yu-Chun (Brad) Chen who spent enormous time with me to discuss my research in details and was willing to share his life experiences. I also thank all my friends for their friendship, help and support, who are Dr. Haitao Zhao, Ms. Huirong Li, Mr. Zhenhong Li, Mr. Ming Zhang and Mr. George Hernandez.

Most of all, I thank my parents, Hsueh-Jung Tsai and I-Min Liao, for their love, encouragement, dedication, and support. I also thank my girlfriend, Yueh-Chuan Liu, who always believe in me, encourage me to try out my own life, and give me all her support whenever I need it. I would like dedicate this thesis to my family.

Table of Contents

List of Figures

List of Tables

Chapter 1

INTRODUCTION

Since the first amazing discovery of carbon nanotubes (CNTs) by Japanese physicist Iijima in 1991 using arc discharge method [1], they have attracted considerable interest because of their extraordinary properties. CNTs are known for their superior mechanical strength, low weight, good heat conductance, and varying electronic properties depending on their helicity and diameter. In particular, the recent research studies [2–4] have reported that CNTs have excellent electrical field emission properties, with high emission currents at low electric field strength. The turn-on voltage of CNTs can be as low as 1-3 V/μm and emission current can be as high as 0.1mA from a single nanotube [5]. As a result, CNT are considered as one of the promising materials as cold-cathode field emission sources, especially for application requiring high-current densities and lightweight packaging.

CNTs are essentially tubes with the diameter of nanometer and made of carbon. One could think of it as a graphene sheet rolled upinto tubes. The structure of a graphene sheet is shown in Figure 1.1 [6], which is a planar sheet of carbon atoms that are densely packed in a honeycomb crystal lattice. CNTs are distinguished by their numbers of concentric layers ("wall"), with spacing $\approx 0.34nm$, and their chirality (wrapping angle). They are typically categorized as single-wall CNTs (SWCNTs), double-wall CNTs (DWCNTs), and multi-wall CNTs (MWCNTs) with respect to the numbers of graphitic layer, as shown in Figure 1.2 [7]. The typical diameter of SWCNTs are 0.4 to 5nm, and MWCNTs can be up to 100nm. The number of sidewalls of CNTs can can be precisouly controlled by the preparation of catalyst that serves as the CNT growth sites that is deposited onto the substrate prior to the growth.

There are two general growth mechanisms that have been proposed [8]. When the catalyst particles remain anchored to the substrate, this is known as "base-growth" model

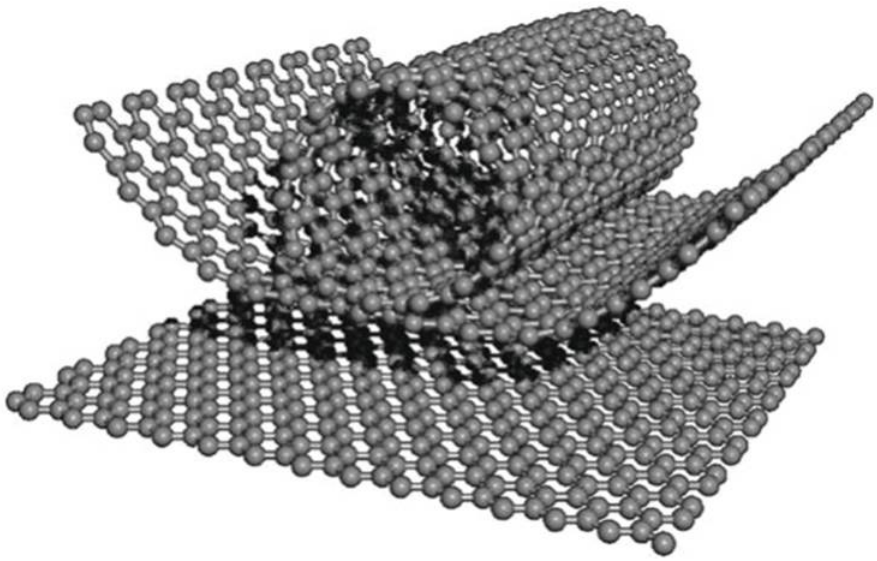

Figure 1.1: Schematic of an individual layer of honeycomb-like carbon called graphene, rolling into CNT [6]

(Figure 1.3 [8]). On the other hand, the growth follows a "tip-growth" model when the metal catalyst particles lift off from the substrate and remain at the top of the CNTs during growth. In both cases, carbon is added at the catalyst site for CNTs to grow.

Currently, there are several synthesis techniques proposed for growing CNTs. These can be divided into methods where CNTs grow from transition metal catalyst particles, and method where CNTs grow without catalyst particles. They include carbon arc discharge [9], laser ablation [10], and chemical vapor deposition [11].

Numbers of potential applications of CNTs have been widely proposed. Among these, CNTs have been reported to be a promosing materials for cold-cathode applications [12]. Because of their high aspect ratio, electrons can be emitted easily from the tips of CNTs in a vacuum ambient under a relatively low applied electric field. Also, the high current density of CNTs is the other important property making them attractive [13].

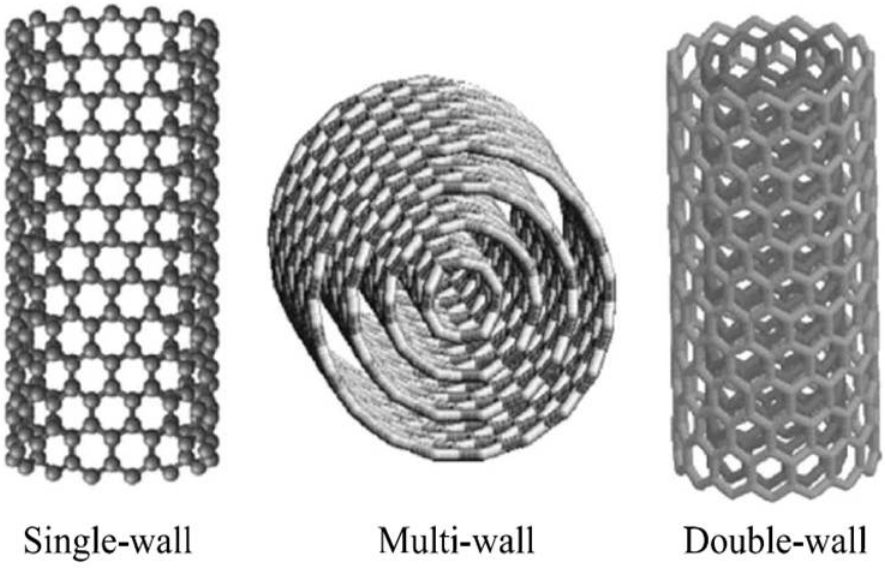

Figure 1.2: Atomic structures of carbon nanotubes [7]

The purpose of this study is to investigating the growth condition of CNTs on different underlaying layers and catalyst types and characterize their field emission properties. From the experimental results, It is found that underlaying layers play an criticle role for CNTs growth. SiO_2, Titanium and Tungsten are used. Each of them has substantially different performances as a substrate for CNTs growth. In addition to investigation of underlayers, the transitation metals, Iron and Cobalt, are utilized as catalysts for depositing CNTs. Randomly-oriented and vertically-aligned CNTs can be grown by controlling the experimental parameters such as catalyst type, catalyst thickness, and deposition temperature. Moreover, different sizes of patterned CNTs are also successfully grown by utilizing basic photolithography steps.

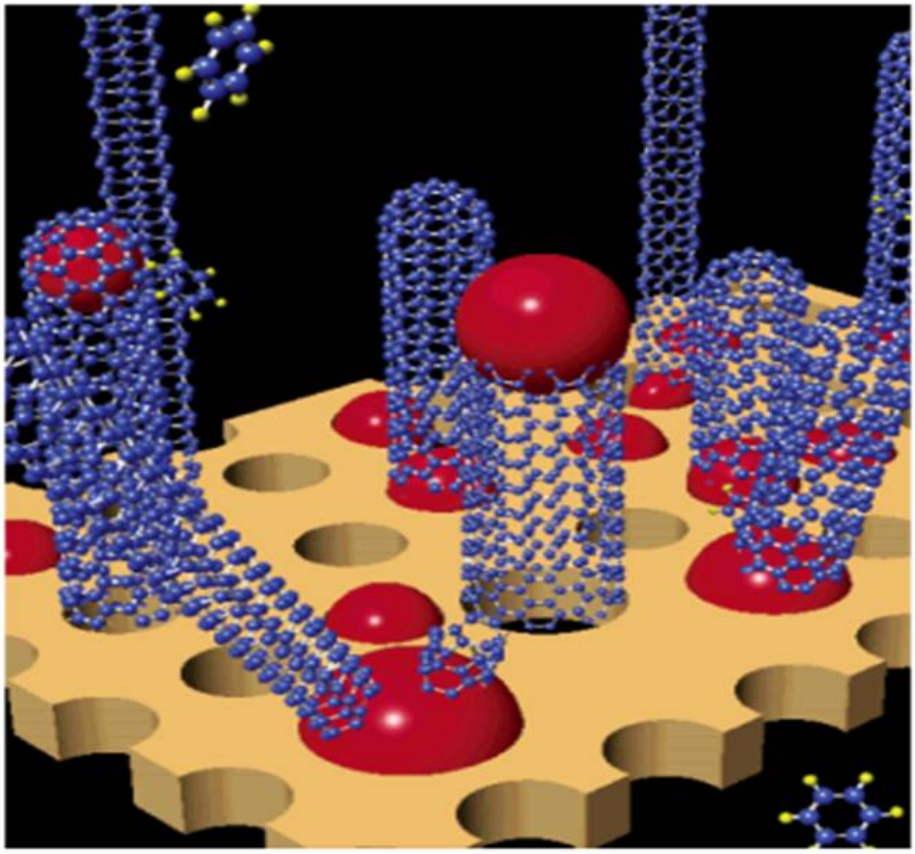

Figure 1.3: Base and tip growth of CNTs rooted in a nanoporous (e.g. zeolite) substrate [8]

Chapter 2

LITERATURE REVIEW

2.1 Material properties of carbon nanotubes

2.1.1 Structure of carbon nanotubes

Carbon, the group IV element, is very active in producing many molecular compounds and crystalling solids. A carbon atom has six electrons which occupy $1s^2$, $2s^2$, and $2p^2$ atomic orbital and can hybridize in sp, sp^2 or sp^3 forms. It has been used for centries, but yet it has been stimulated in the nanotechnology field by the discovery of these unique nanometer sizes of sp^2 carbon-bonded materials such as fullerene, carbon nanotube and graphite, as shown in Figure 2.1 [14].

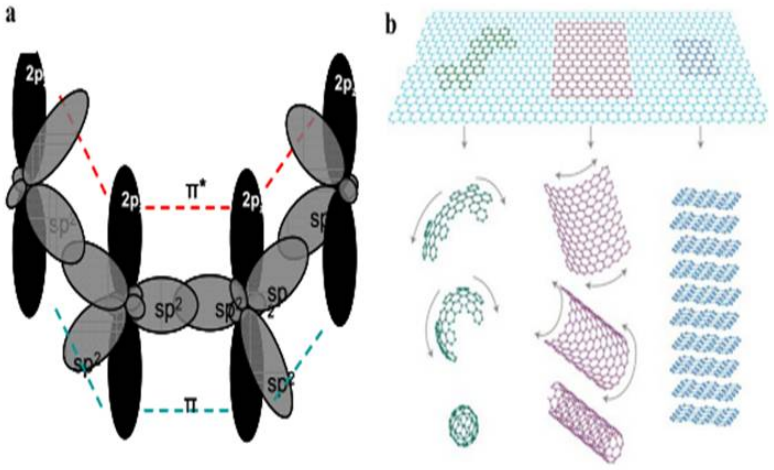

Figure 2.1: sp^2 hybridization of carbon and its derived materials. (a) The three sp^2 hybridized orbital are in-plane, with 2p orbital orthogonal to the plane, π and $\pi^\star$ denotes the bonding and anti bonding orbital. (b) Graphene as the source of three different materials, fullerence (left), carbon nanotube (center) and bulk graphite (right) [14]

Carbon nanotube (CNT), a new form of pure carbon, can be thought as a hexagonal graphene sheet rolled up to form a cylinder that is capped by pentagonal carbon rign. Depending on the manner in which the graphene sheet is rolled up, the arrangement of carbon atoms along the cylinder circumference can be “arm-chair”, “zig-zag”, or several different intermediate chiral structure (Figure 2.2) [15].

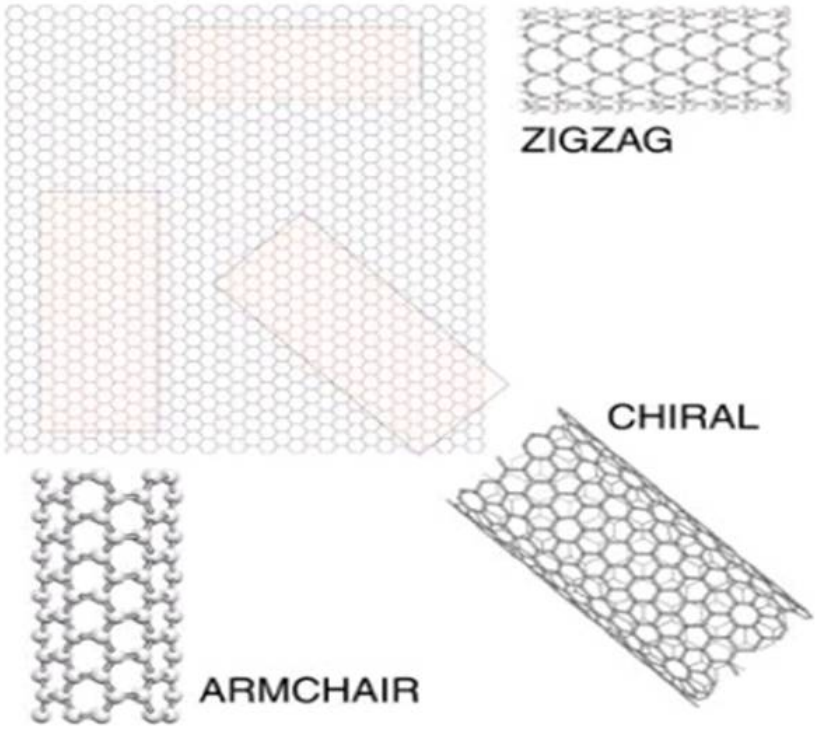

Figure 2.2: Chiral structure of carbon nanotube [15]

CNTs are distinguished by their numbers of concentric layers called the ”walls”, with spacing of sub-nm, and their chirality. There are several types of CNTs: Single-Wall CNTs (SWCNTs), Double-Wall CNTs (DWCNTs), and Multi-Wall CNTs (MWCNTs) with respect to the number of graphitic layers (Figure 1.2). Unlike graphene, CNTs exhibit different physical properties depending upon their structure. The crystal structure of a nanotube depends upon the axis along which the cylinder is formed from the graphene sheet. Figure 2.3 [16] shows the vectors on graphene plane that are important in understanding the formation of

a nanotube . Here, we will follow the established notations, which can be found in literature [17]. The electrical character of a nanotube is specified by two numbers that determine the chirality of the nanotube. The vector OB perpendicular to the nanotube axis is called chiral vector $\overrightarrow{C_h}$. The vector OA, which is parallel to the axis is termed as the translational vector T, this is the unit vector of 1-D nanotube. The chiral vector is $\overrightarrow{C_h} = \mathrm{n}\overrightarrow{a_1} + \mathrm{m}\overrightarrow{a_2}$ and the chiral numbers n and m are integers (the chirality convention requires $0 \leq |m| \leq$n). The length of the unit vectors is a and the angle they enclose is 60°. As a result, the diameter of the nanotube can be expressed as:

$$\mathrm{d} = \frac{\overrightarrow{C_h}}{\pi} = \frac{a\sqrt{m^2 + mn + n^2}}{\pi}$$

and the chiral angle from the figure with the expression:

$$\cos\theta = \frac{\overrightarrow{C_h}\overrightarrow{a_1}}{\mid \overrightarrow{C_h} \mid\mid \overrightarrow{a_1} \mid} = \frac{2n + m}{2\sqrt{n^2 + m^2 + nm}}$$

Due to the hexagonal symmetry of the lattice, the chiral angle can only take on values between 0 and 30°. The electron wavevector along the circumference of the CNT is quantized while the graphene sheet is rolled. It is shown that this condition leads to a metallic nanotube, zero band gap, when the difference n-m is a multiple of 3 [17].

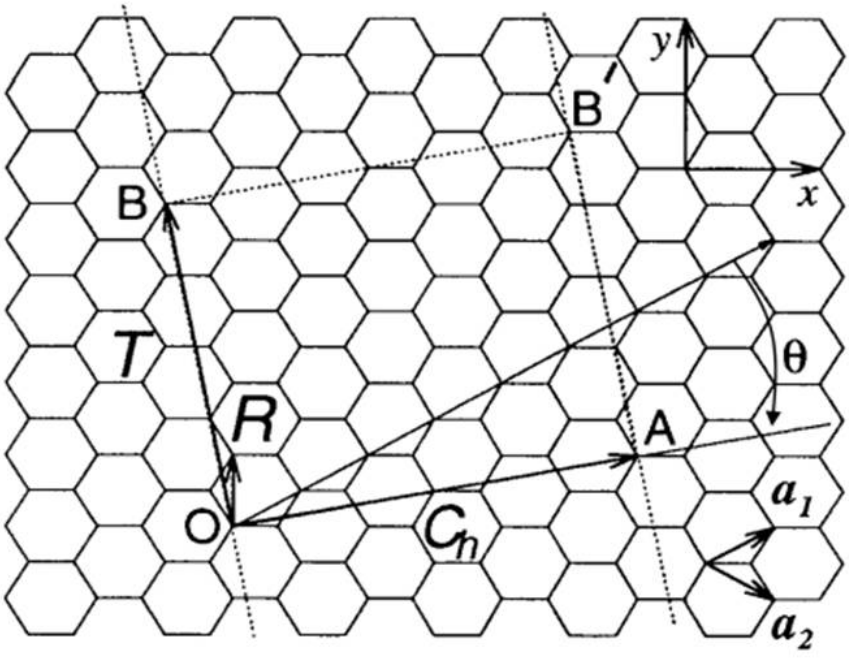

Figure 2.3: A two-dimensional honeycomb lattice of graphene sheet. The vectors OA and OB define the chiral vector C_h. Unitary vector a_1 and a_2 are to determine the rolling direction expressed by vector C_h. There are several ways to roll it up As a result, different types of tubules can be formed [16].

2.1.2 Electrical properties

CNTs can be either metallic or semiconducting depending on the configuration and molecular structure [18]. For example, SWCNT is metallic if the structure is armchair. On the other hand, zigzag tube as well as chiral-type tube (m,n) with 2m+n=3N (N: positive integer), is a narrow-gap semiconductive [19]. In contrast, the band structures of MWCNTs are more sophisticated because of the interlayer coupling. However, theoretical discussion by Saito et al. emphasized that the interlayer has little effect on the electronic properties of individual tubes [20]. As a result, two coaxial armchair nanotubes yield a DWCNT. Coaxial metallic-semiconducting and semiconducting-metallic tube will retain their respective characters when interlayer interaction is introduced [19].

Several techniques have been utilized in determining the properties of CNTs, such as raman spectroscopy [21], electron energy loss spectroscopy (EELS) [22], electron spin resonance (ESR) [23], scanning tunneling microscopy (STM) [24], four-point probe, and atomic force microscopy (AFM).

Many groups worked on characterizing the conductivity of CNTs. Ebbesen et al [25] measured the resistivities of MWCNTs using four-point probe technique and determined the resistivties of nanotubes ranged between 8mΩ-m and 0.051 $\mu\Omega$-m. The results show that the electrical resistivity of CNTs can vary greatly according to their porposed structure. The resistivity of SWCNTs have also been measured by means of four-probe arrangement by Smalley et al. [26], and ranged from 0.34$\mu\Omega$-m to 1.0$\mu\Omega$-m. The range of resistivities for SWCNTs is smaller than MWCNTs because it is not very conductive between the multilayers of MWCNTs.

2.1.3 Mechanical properties

CNT are among the strongest materials in nature, especially in the axial direction. Because of their high strength-to-weight (STW) ratio, CNTs have been concluded as one of the stiffest materials. Also, traditional carbon nanofibers have the the STW ratio of 40 times

greater than steel, however, CNTs have STW ratio at least 2 orders of magnitude greater than steel [19]. According to Lourie et. al [27], SWCNTs have Young's modulus of 2.8 - 3.6 TPa, and MWCNTs for 1.7 - 2.4 TPa. In addition, direct tensile loading tests of SWCNTs and MWCNTs have been reported by Yu et al [28] . The Yong's modulus can be obtained ranging from 320 to 1470 GPa for SWCNTs and from 270 to 950 GPa for MWCNTs [17]. Theoretical studies have suggested that SWCNTs have Young's modulus as high as 1 - 5 TPa [29]. For MWCNTs, the strength would be affected by the sliding of individual graphene cylinders with respect to each other. Treacy et al. [30] were the first to report fitting Young's modulus of MWCNTs to experimental data. For a total of 11 MWCNTs' Young's modulus values were reported as ranging from 0.4 to 4.15 TPa with a mean of 1.8 TPa. A similar experimental research on SWCNTs was reported by Krishnan et al [31], who presented an average Young's modulus of 1.3 TPa from measured amplitudes of 27 SWNTs.

2.1.4 Other properties

In addition to the electrical and mechanical properties, there are other outstanding properteis that make CNTs attractive such as optical properties, high thermal conductivity ,and high resistance to chemical attacks. As a result, CNTs can be applied on a variety of technological applications. For example, the researchers shows that the low-density vertcially aligned CNTs arrays can be engineered to have an extremely low index of refraction and combined with the nanoscale surface roughness of the arrays , can produce a near-perfect optical absoprtion materials [32]. Moreover, CNTs have been demonstrated that can be the fabricated as the darkest materials. [33]. As a result, CNTs will be the excellent candidate as the next-generation solar cell materials.

2.2 Synthesis techniques of carbon nanotubes

Currently, CNTs can be synthesized by using a variety of techniques such as arc-discharge, laser ablation, chemical vapor depsotion, plasma-enhanced CVD, and so on. In this section, the methods to produce MWCNTs and SWCNTs are summarized.

2.2.1 Arc discharge and laser ablation

Arc discharge and laser ablation methods for growing CNTs have been widely pursued in the past years. Both synthesis techniques are based on condensing carbon atoms from evaporation of solid carbon sources onto substrate. Temperatures in both methods are close to the melting temperature of graphite, $3000 - 4000\,^{\circ}\mathrm{C}$.

In arc-discharge method, carbon atoms are evaporated by plasma of helium gas ignited by high currents passed through opposing carbon anode and cathode. The arc-discharge technique has been developed into an excellent method for producing both high quality MWCNTs and SWCNTs. In 1992, the DC-arc technique was first done by Ebbesen et al. [34] and become a common scientific method for synthesizing MWCNTs. MWCNTs have lengths of on the order of ten microns and diameter in the range of 5 - 30nm. A schemtaic diagram of DC arc-discharge method used for synthesizing CNTs is shown in Figure 2.5 [16]. The arc is generated between two pure graphite electrodes. The positive electrode must be replaced with a new one before doing any new deposition because it is consumed in the arc. Helium is a typical gas used as filling up the chamber because it has low ionization potential. It flows though the chamber from the inlet a at a desired pressure of around 500 torr. Since plasma is necessary in this methode, the type and pressure of the gas surrounding the arc becomes critical. The typical applied DC voltage is 20 V. The positive electrode is brought closer to negative one until arcing occurs. A plasma with a temperature up to $3700\,^{\circ}\mathrm{C}$ is formed. Consequently, the variation of temperature might cause the large size distribution of CNTs. The deposit forms on the negative electrode where there is a current flowing. It

has been shown that lower the current flow, the better the yields of CNTs are. With this process, a following purification procedure is needed to extract CNT samples [35].

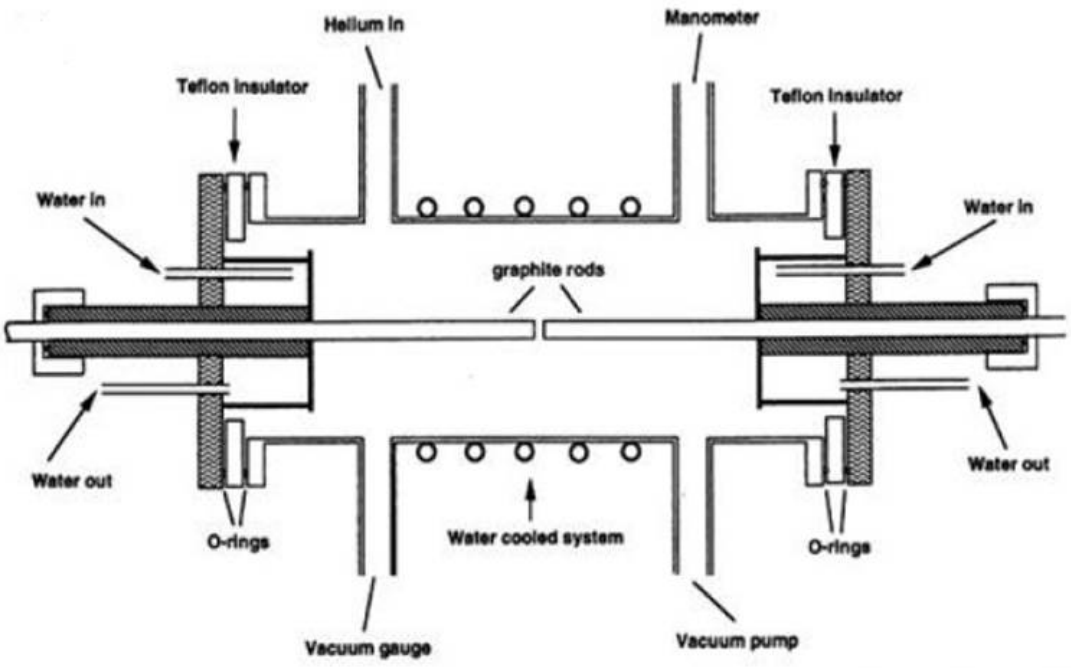

Figure 2.4: Schematic diagram of the arc apparatus where the nanotubes are formed from the plasma between the two carbon rods [16]

The growth of high-quality SWCNTs at the 1 - 10g scale was achieved by Smalley using a laser ablation method. The schematic diagram is shown in Figure 2.6 [36]. The method took advantage of intense laser pulses to ablate a carbon target which contains 0.5 atomic percent of nickel and cobalt. The target was palced in a tube-furnace heated to 1200 °C. During the processing of laser ablation, a flow of inert gas was passed through the chamber to carry the grown nanotubes downstream to be collected on a cold finger. The synthesized SWCNTs are mostly in the form of ropes consisting of tens of individual nanotubes close-packed into hexagonal crystals via Vander Waals interactions. In growth SWCNTs by means of arc-discharge and laser ablation, typical by-products including fullerenes, graphitic polyhedrons with enclosed metal particles, and amorphous carbon in the form of particles or overcoating on the sidewalls of nanotubes have been seen [17].

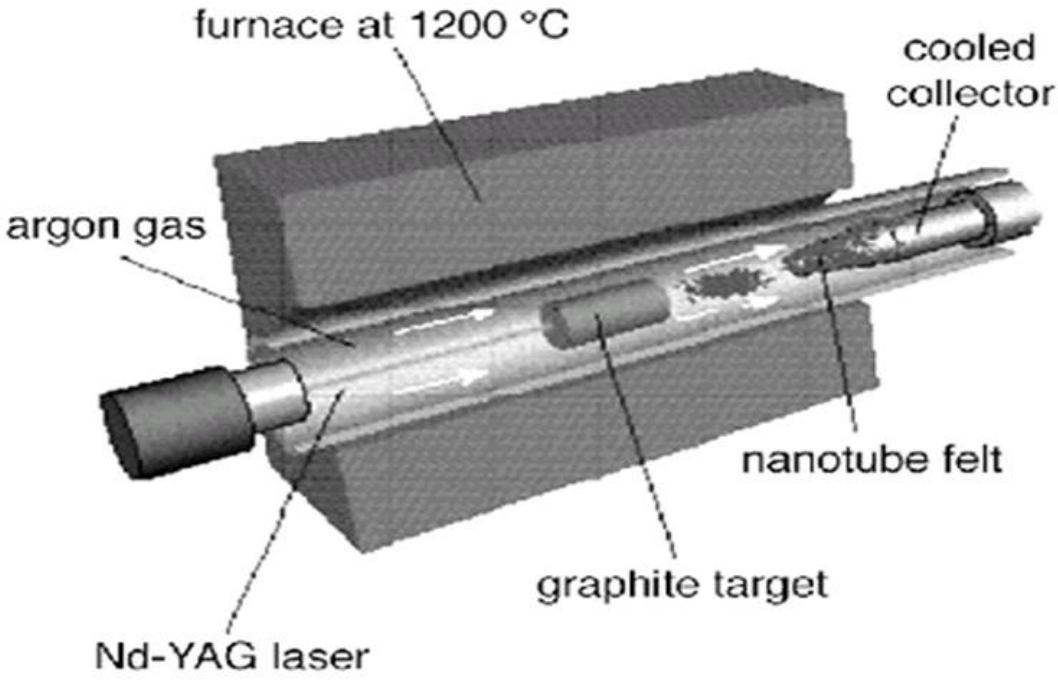

Figure 2.5: Schematic diagram of a laser ablation set-up [36]

2.2.2 Chemical vapor deposition

Among these synthetic techniques, chemical vapor deposition (CVD) method is especially attractive because it can be easily scaled up. The synthesis of CNTs by CVD method requires the presence of a gaseous phase activated carbon. It is common to use gaseous carbon sources including methane, acetylene, and carbon monoxide. But also alcohols and carbon clusters derived from solid carbon forms can be used. The activation of the molecules or of the nanostructured fragments is achieved using a variety of methods which can be roughly categorized as: [37]

1) *Plasma CVD*
2) *Thermal CVD*

CNTs synthesis by CVD is a two-step process consisting of a preliminary catalyst preparation step followed by actual synthesis of the nanotubes. In general, CVD technique tends to produce nanotubes with fewer carbonaceous impurities with respect to the other synthetic techniques and the residual particles of the metal catalyst are frequently found at an extremity of the nanotube, making their elimination by post-synthesis chemical processes easier. The choice of metal cayalyst, usually a first-row transition metal such as Ni, Fe, or Co can drive the process toward the preferential growth of single rather than multiwall nanotubes and to control the formation of individual or bundled nanotubes. The dimensions of the catalyst are very important: large particles can produce MWCNTs, but if the particle size of the metal or metallic alloy is too large, carbon filaments or fibers can be produced instead of nanotubes [37].

In plasma enhanced CVD technique, the plasmas is used to decompose and activate the reactants in the gas phase. Plasma is often generated by hot-filament or by electrical discharges at different frequencies (DC, RF, MW). Plasma-enhanced CVD (PECVD) is a method that can be easily scaled-up. In PECVD, the catalyst is supported by the substrate

and can be prepared by wet chemistry or by a sputtering process. In the first case, a solution containing a metal compound is deposited by casting onto the substrate surface. In the second case, a layer of metal is deposited on the substrate by sputtering. Both processes are followed by either chemical etching or thermal annealing to induce catalyst clustering and particle formation on the substrate. The reactive carbon species in the gas phase then diffuse towards the substrate, which is generally heated between 650 to 1500 °C temperature. The pressure in the deposition reactors is typically low ($<$ 100 Torr).

In a hot filament reactor, the reactants are activated by a heated filament that induces the formation of radicals and active species: the reaction product condense on a substrate forming a deposit. The fundamental components of a typical hot filament CVD (HFCVD) system for the growth of nanotubes are: 1) A vcauum chamber that the pressure of the reaction gases is maintained at values between 10 and 300 Torr. 2) A heated filament located at a distance of a few mm from the substrate on which the material must be deposited. 3) An additional system for heating the substrate up to $800 - 1500\,^{\circ}\mathrm{C}$.

The thermal CVD method involves the decomposition of a gaseous or volatile compound of carbon, catalyzed by metallic nanoparticles, which also serve as nucleation sites for the initiation of nanotube growth. Abundant carbon gas mixed with argon or nitrogen gases are used, but sometimes the starting material can be a liquid that is consequently vaporized. The catalyst can be either in solid form, supported on a previously coated substrate, or mixed with the feed gas, and flowed into the reactor. The deposition reactors are typically maintained under atmospheric pressure, even if some intereting processes can be carried out under high-pressure condition. It has the advantage of being remarkably cheap and offer the posibility of being easily scaled-up. One disadvantage is the presence of deposits of a large amount of residual metallic catalyst. The general scheme of a thermal CVD apparatus for carbon nanotubes synthesis is shown in Figure 2.8 [38].

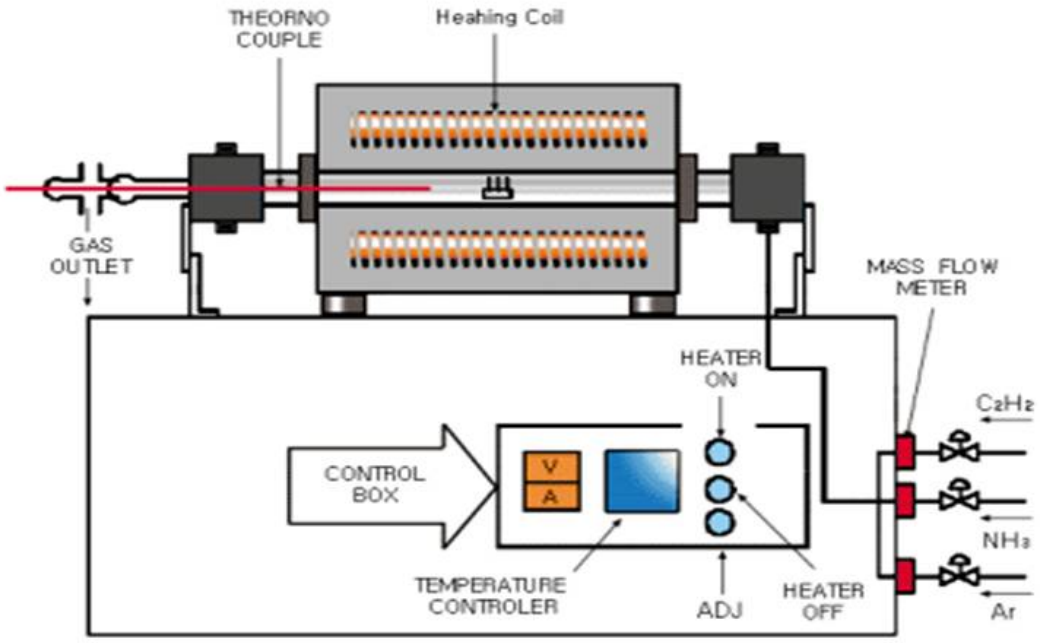

Figure 2.6: Schematic diagram for thermal CVD reactor [38]

In thermal CVD, the catalyst has a strong effect on the growth rate and on the final nanotube yield [39]. Therefore, various techniques have been developed for the preparation of catalyst. It is often used in bulk quantities, and to the choice of a suitable catalyst support. For example, the use of metallic alloys to catalyze for the nanotube growth often results in an enhancement of the yields. Nanoparticles of bimetallic alloys, as for exmple Fe and Co, give 10 - 100 times higher yield of SWNTs than pure Fe [40]. The effect of deposition temperature and of the metal particle concentration on the deposit morphology has also been investigated [41]. When growing CNTs by thermal CVD on a catalyst supported by a substrate, the CNT diameters are often found to be dependent on the film thickness or on the particle size. For instance, a research group reported [42] that using substrates coated by a metal film with a thickness of 13 and 27nm, the diameter distribution resulted in the ranges of 30 - 40 nm and 100 - 200 nm respectively.

2.3 Growth mechanisms of CNTs

Growth mechanism is always an interesting topic that has been debatable right from its discovery. Several research groups have reported a variety of possibilities which are often contradicting. As a result, there is no well established CNT growth mechanism. However, there are two widely accepted mechanism can be categorized as tip-growth model and base-growth model. Hydrocarbon vapor when comes in contact with the hot metal nanoparticels, first decomposes into carbon and hydrogen species; hydrogen flies away and carbon gets dissolved into the metal. After reaching the carbon-solubility limit in the metal at that temperatutre, as-dissolved carbon precipitates out and crystallizes in the form of a cylindrical network having no dangling bonds [43]. When the catalyst-substrate interaction is weak, hydrocarbon decomposes on the top surface of the metal; carbon diffuses down through the metal; and CNT precipitates out across the metal bottom, pushing the whole metal particle off the substrate. This is described in picture 2.9 (a) As long as the metal's top is open for fresh hydrocarbon decomposition, CNT continues to grow longer and longer. Once the metal is fully covered with excess carbon, its catalytic activity ceases and the CNT growth is stopped. This is known as tip-growth model (Figure 2.9(a) [43]).

On the other hand, when the catalyst-substrate interaction is strong, initial hydrocarbon decomposition and carbon diffusion take place similar to that in the tip-growth case, but the CNT precipitation fails to push the metal particle up; so the precipitation is compelled to emerge out from the metal's apex. First, carbon crystallizes out as a hemispherical dome which then extends up in the form of seamless graphitic cylinder. Subsequent hydrocarbon deposition takes place on the lower peripheral surface of the metal, and as-dissolved carbon diffuses upward. CNT grows up with the catalyst particle rooted on its base; hence, this is known as base-growth model (Figure 2.9(b) [43]). CNT synthesis involves many parameters such as hydrocarbon, catalyst, temperature, pressure, gas flow rate, deposition time and reactor geometry.

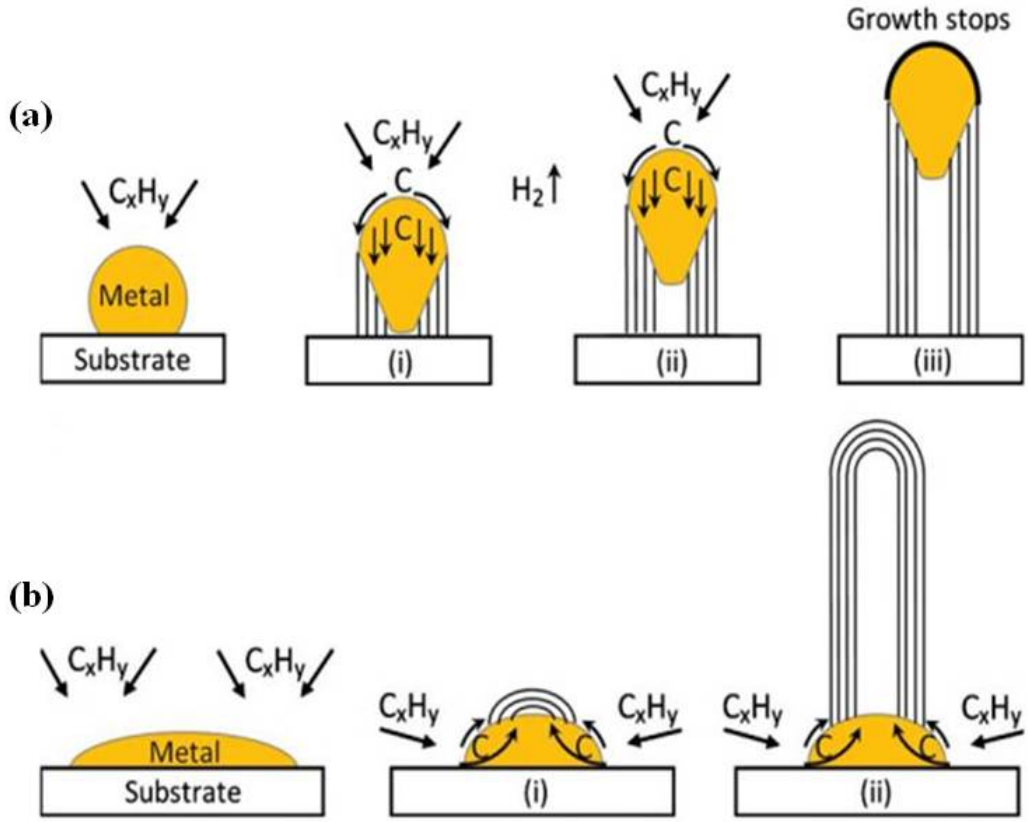

Figure 2.7: (a) tip-growth model (b) base-growth model [43]

2.4 Field emission of electrons from CNTs

Local electric field is the field that surface experiences and proportional to the applied field, when applied field is enhaced due to "sharp" surface irregulation. Field emission is a process that the electrons are emitted from a cold solid surface under the action of a strong electric field. It involves the extraction of electrons from a solid by tunneling through the surface potential barrier. The potential barrier is square when no electric field is applied as shown in Figure 2.8 [44]. Its shape becomes triangular when a negative potential is applied to the solid, with a slope that depends on the amplitude of the local electic field, F, just above the surface. Field emission from CNTs follows the same physics. For a single nanotube with sharp tip, the local electic field cannot be simply calculated by dividing the applied voltage

by the gap distance between the tip of the nanotube and the anode electrode. The local field will be higher by a factor β, which amplifies the field and is determined by the geometrical shape of the emitter. Therefore, the electric field is written as: $F = \beta E = \beta V/d_0$, where E is the applied field. The field emission characteristic of SWCNT have been studied [45]. Most single SWCNT emitters with a closed tip as well as opened are capable of emitting over an incredibly large current. Field emission from individual MWCNTs has studied by Satio et al [46]. Also, they have used closed and opened tubes as the sources in a field emission microscopy. The motivation behind these studied is to explore the possibility of using individual nanotube field emitters in cathod ray tubes or electron guns for electron microscopy.

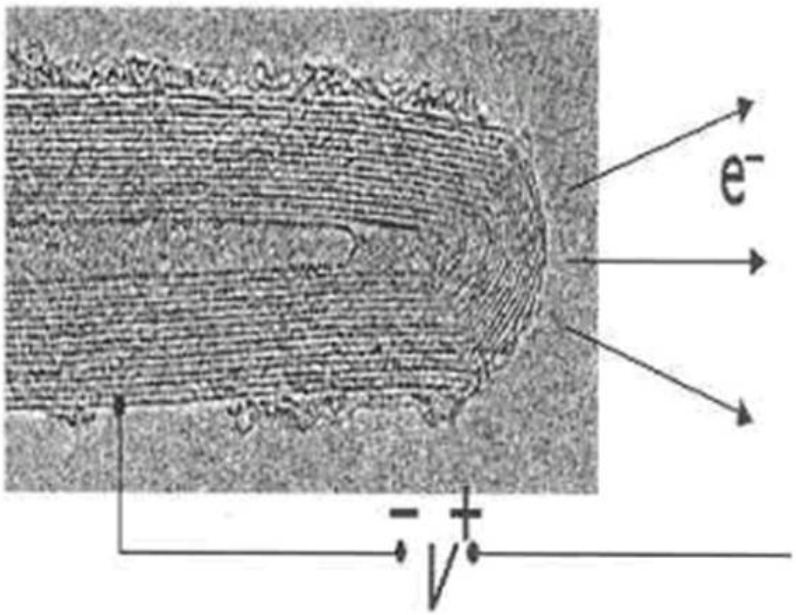

Figure 2.8: Typical set-up for field emission: a potential difference is applied between a nanotube and a counter electrode [44]

The emission current increases linearly with applied field for a field smaller than a critical field which is designated as the turn-on field, E_0, and then the current increases exponentially with the applied field for a field stronger than turn-on field. The J-E characteristics of the CNTs were analyzed using Fowler-Nordheim (F-N) model [47]:

$$J{=}a\ E^2\ \exp\Big(\frac{-b}{E}\Big),\ \text{where}\ a{=}\frac{A\alpha\beta^2/d^2}{1.1\phi}\exp\Big(\frac{1.44\times10^{-7}B}{\phi^{1/2}}\Big),\ b{=}\frac{0.95B\phi^{3/2}d}{\beta}$$

, where A is $1.54{\times}10^{-6}$ eV V^{-2} and B is 6.83 $\times10^7$ $eV^{-3/2}V\ cm^{-1}$ derived from quantum statistics, ϕ is the work function of CNTs, α is the emission effetive area, and β is the field enhancement factor, which is directly related to the geometry and surface properties of the CNT samples. The applied electric field is defined as $E{=}V/d$, where V is the applied voltage and d is the distance between the electrodes. The localized electric field experienced by one CNT is expected to be $\beta V/d$. The parameters in the F-N equation can be deduced by fitting the $\ln(\mathrm{I}/V^2)$ vs. 1/V curve, the F-N plot. Fowler-Nordheim model shows that the dependence of the emitted current on the local electric field E and the work function ϕ, is exponential like.

2.5 Potential applications of CNTs

Many potential applications have been reported for CNTs including their use as reinforcement in composite materials, as transparent and flexible electrodes [48], AFM/STM tips (Figure 2.9 [49]), and electron-field emitters [50]. The SWCNT films can exhibit conductivity/transmittance values comparable to those of low-temperature ITO. Transparent conducting SWCNT coatings on flexible substrates such as polyethylene terephthalate (PET) outperform ITO/PET electrodes in terms of chemical and mechanical stability and exhbit a wider electrochemical window. Moreover, the application of SWCNTs as field-emission electron sources for use in flat-panel displays [17], gas-discharge tubes [17] and microwave generators [51] has been widely explored. The advantages of these devices over those made from metals such as tungsten and molybdenum are the following: relatively easy manufacturing/fabrication process, less deterioration in high vacuum (10^{-8}Torr), and high current

densities of 10^9 A/cm^2. Other desirable properties that make CNTs promising materials as field emitters are their nanosize diameter, structural integrity, high electrical conductivity, and high chemical stability. Studies on a field-effect transistor (Figure 2.10 [52]) made from a semiconducting SWCNT showed it to have the ability to be switched from a conducting to an insulating state. Logic switches, the basic components of computers, can be constructed by coupling such CNT transistors. Recently, the application of random CNT Networks (CNTNs) as semiconducting materials for thin-film transistors (TFT) [53] has attracted interest due to their superior performance compared to that of organic TFTs and potentially low-cost fabrication. Uniformity of CNTN properties is achieved by statistical averaging over the large number of individual tubes that make up the network. Various devices and components based on CNTNs have been successfully demonstrated, including diodes, logic circuit elements, solar cells, displays, and sensors [53].

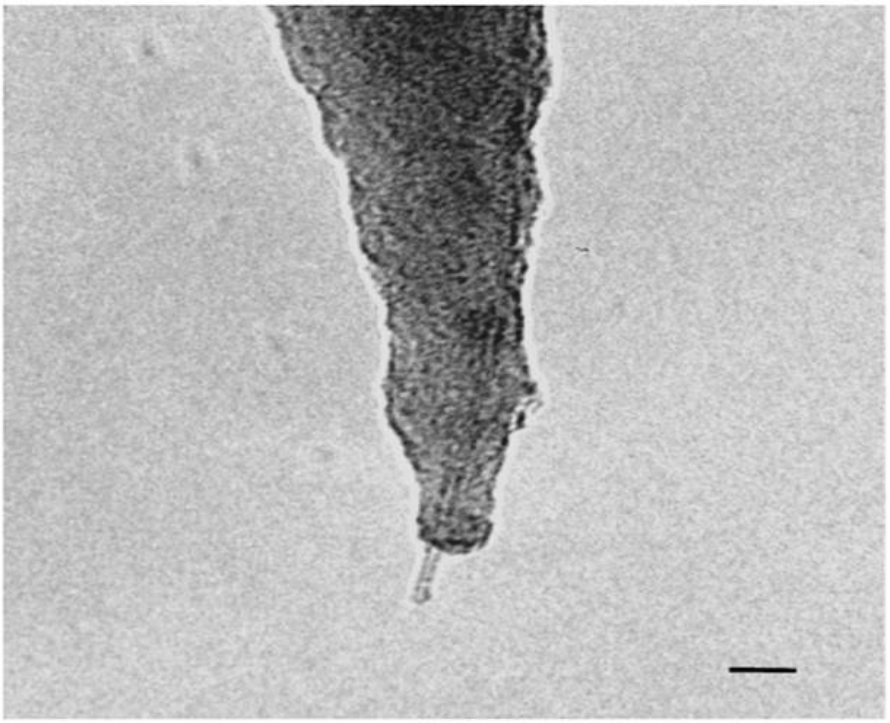

Figure 2.9: TEM image of an individual SWNT tip produced by controlling carefully the catalyst density. The scale bar equals 10 nm [49]

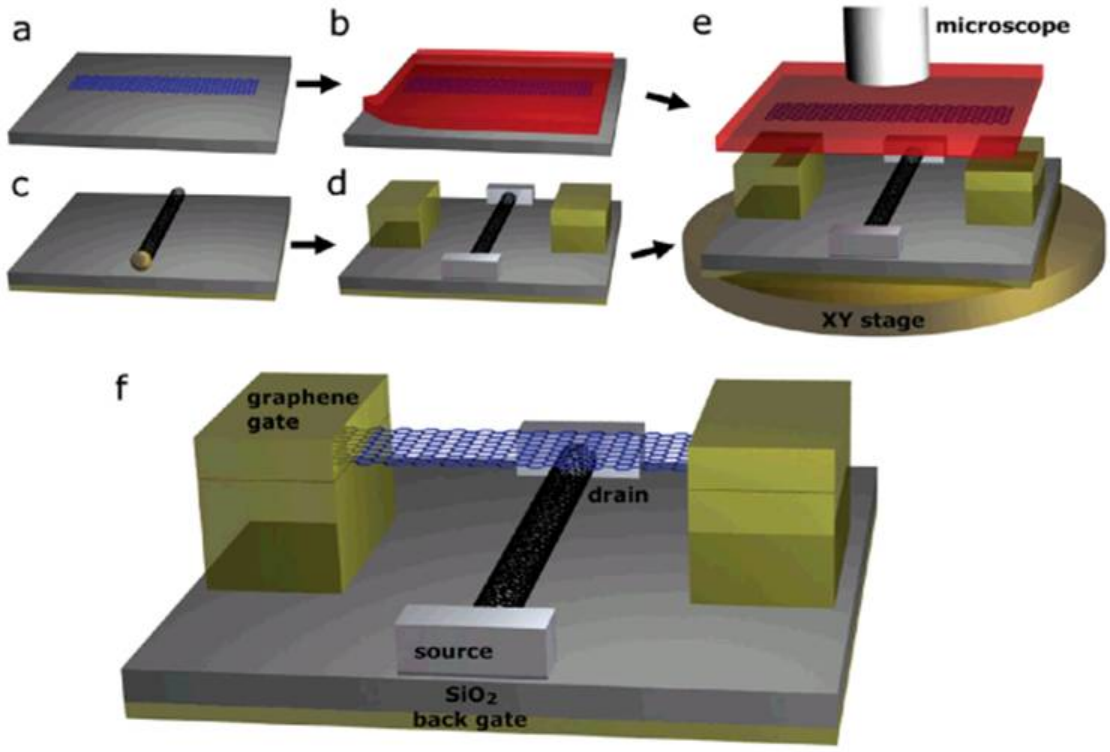

Figure 2.10: Schematic process for the fabrication of a CNTFET with a suspended graphene gate without any Si3N4 protective layer: The CNTFET can be gated either by the suspended graphene gate or by the Si substrate acting as a back gate [52].

Chapter 3

Carbon Nanotubes: FABRICATION AND CHARACTERIZATION

In this study, CNTs are synthesized using thermal chemical vapor deposition technique (CVD). The CVD method has advantages of simple equipment setup and excellent uniformity of thin-film deposition over large area. Silicon wafers are used as the substrate for CNTs growth and several underlayers and catalyst materials deposited on the silicon wafers using DC/RF magnetron supttering system. Once the synthesis process is completed, CNTs are examined used scanning electron microscopy (SEM) and their electrical properties are characterized by field emission measurements in vacuum. Synthezied parameters are optimized by using sputtering and growth conditions.

3.0.1 Growth process

Two metal catalysts were used. Fe as the catalyst, the growth of CNTs is carried at a temperaute of 700 °C, however, Co as the catlyst, the temperature was risen from 700 to 850 °C. All the experiments were running at the pressure of 70 Torr and the growth time are all 20 min. Figure 3.1 shows the schematic diagram for the thermal CVD reactor used for the growth of CNTs. A resistive heater is used to heat the quartz substrate inside the furnace. A thermocouple is connected to the substrate holder to measure the temperature. Flowmeters connected between the chamber and the gas cylinders are used to measure the gas flow into the CVD chamber. The pressure in the chamber is controlled by a throttle valve, which is connected between mechanical pump and the pressure gauge. The gas mixture of acetylene and argon with 20 and 75sccm respectively were used as the feed gas in the chamber. For growing the vertically-aligned MWCNTs (VA-MWCNTs), after the deposition of the iron catlayst, it was received the other graphite deposition. After two steps deposition processes,

the sample was oxidized in air at 300 °C for 8 hours. Thermal CVD of CNTs was performed in a vacuum furnace filled with a gas mixture of acetylene and argon at a pressure of 70 torr. Before the gas mixture was fed into the furnace, the substrate was heated to 700 °C in vacuum and the temperature was remained constant during the 20 min growth of MWNTs. VA-MWNTs grew on the substrate iwht a uniform length approximately 20 μm (Figure 4.8).

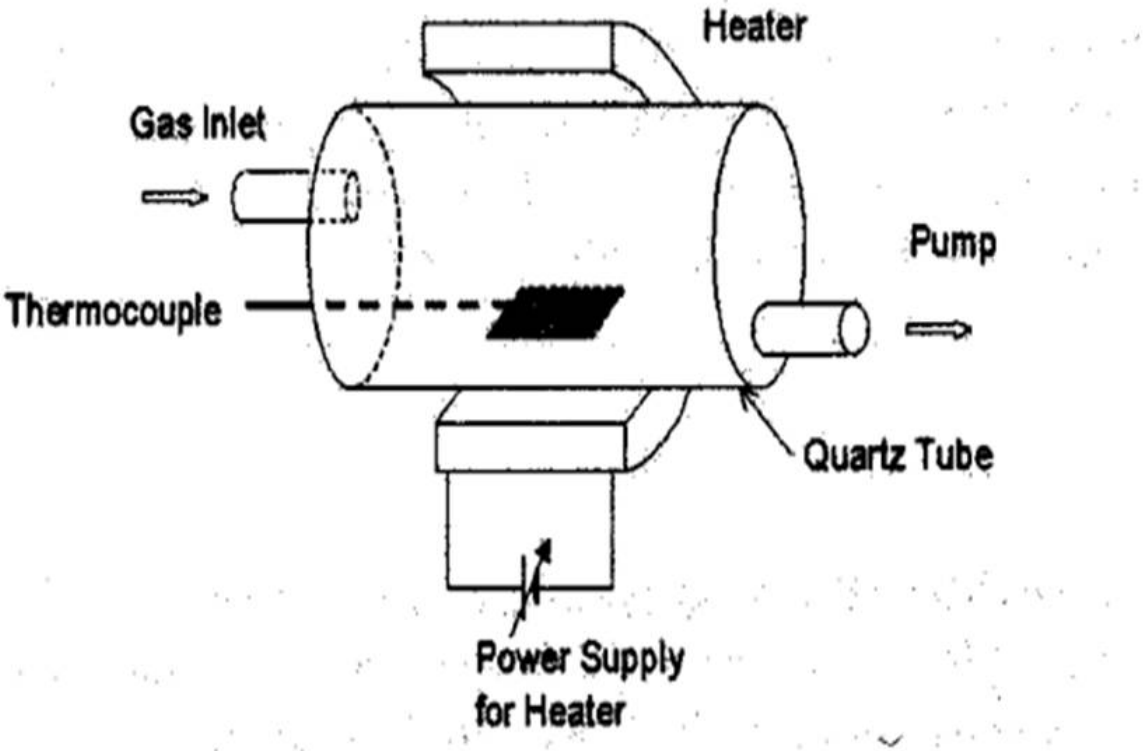

Figure 3.1: Schematic diagram for thermal CVD reactor [54]

3.0.2 Selective grown CNTs synthesis processes

The fabrication process for synthesizing selectively grown CNTs sample is carried out in detail as shown in Figure 3.3. First, the plain n-type (100) silicon wafers are cleaned by the standard RCA (Radio Corporation of Americ) cleaning procedure. They are dipped into a Buffered Oxide Etching (BOE) solution in order to remove native oxide and chemical impurities, followed by deionized water (DI water) rinse for a couples of minutes. A dehydration bake step for 20min is performed before priming and spin-coating a wafer with resist. Following the dehydration bake, the silicon wafer is primed with a pre-resist coating of a material designed to improve adhesion in this case. Hexamethyldisilazane (HMDS) enhances the adhesion between the Si wafer and the photoresist (PR), and bahaves as surface-linking adhesion promoter. 10min of HMDS priming allows good adhesion. Following cleaning, dehydration baking, and priming, the silicon substrate is coated with photoresist (PR) at a speed of 3000 rpm for 30 sec, and soft-baked on the hotplate at 105 °C for 1min. After a wafer has been coated with resist, it is subjected to a temperature step, called soft-bake (or pre-bake), and it is ready to be exposed to some form of radiation in order to create a latent image in the resist. After exposure, then, the patterned substrate is subject to another temperature step, called hot-bake, putting on the hotplate at 120 °C for 1min. After this baking process, the substrates are then sputtered with iron forming a 7nm thick Fe (purity 99.99%) catalysis film in a sputtering vacuum chamber. The sputtering system is a 2-inch DC magnetron sputtering system with a power 100W through shadow masks, containing different patterned openings with the sizes of 25 m to 0.5 cm at pitch distances of 25 m to 0.5 cm. When the catalyst are deposited onto the substrate, it is dipped into the aceton for couple minutes to remove PR, then the patterned film are successfully obtained.

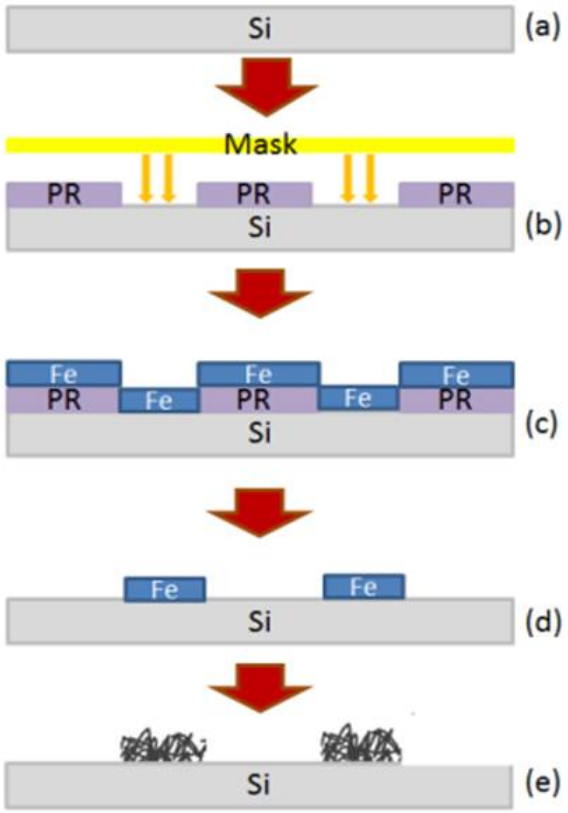

Figure 3.2: Schematic diagram of CNTs fabrication processing (a) silicon wafer cleaned and prepared, (b) mask is aligned to remove parts of the photoresist for patterned deposition of the iron catalyst. (c) the spattering process is conducted. (d) photoresist is removed from the wafer exposing only the sections with catalyst Fe. The sample is now ready to be moved to the CVD chamber for CNT growth process. (e) the CNTs are selectively grown on the substrate.

3.1 Electron field emission measurements and experimental setup

Once the growth process of the CNTs is completed, field emission properties are measured in vacuum. These CNTs samples, one at a time, are loaded into a high vacuum chamber. The chamber is pumped by a turbomolecular pump to a vacuum level of 3×10^{-6} Torr. The measurements are performance at room temperature. The distance between the CNTs sample (the cathode) and the anode is maintained constant by a glass spacer with a thickness of $140\mu m$. A rod made by tungsten with a diameter of 0.4 cm was used as the anode. A dc variable high-voltage supply is used to bias the electrodes. The voltage is continuously increased with intervals between the cathode and the anode. The emission current was recorded by a Keithley picoammeter which was connected to a computer through GPIB card. The applied voltage and the field emission current are recorded and then analyzed. A schematic diagram of an experimental setup used for theses measurements is shown in Figure. 3.3 [6].

For the field emission study, once the voltage and current data are collected, the electric field and the current density data are calculated from the raw data with the following equations:

$$E = \frac{V - IR}{d} \text{ and } j = \frac{I}{S}$$

where R is the resistance of the current limiting resistor with a value of 3 MΩ, d is the gap distance, which is the thickness of the glass spacer, and S is the emission area which is the exposed area of the collector rod to the CNTs. In these equations $d = 140\ \mu m$ and $S = 0.0316\ cm^2$ are used. For each applied voltage, five current data with 1 second intervals are recorded and then averaged to form one data point, to assure the test accuracy.

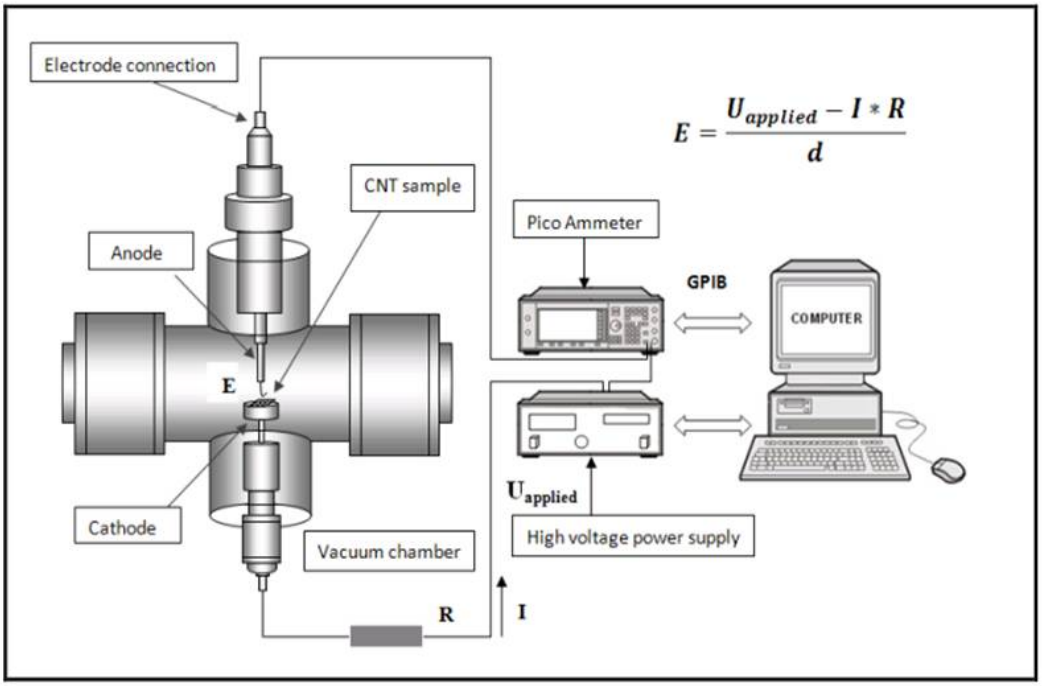

Figure 3.3: Schematic diagram for the field emission measurement setup [6]

Chapter 4

RESULTS AND DISCUSSION

Two different morphologies of CNTs, randomly oriented and vertically aligned, were successfully deposited on silicon substrate with different catalysts and underlying layers by thermal chemical vapor deposition. The catalysts are Iron (Fe) and Cobalt (Co) and underlying layers are SiO_2, Titanium (Ti) and Tungsten (W). The field emission characteristics of the CNTs specimens are examined in a high pressure vacuum chamber. The effect of catalysts and underlying layers on the field emission characteristics of CNTs are studied.

Table 4.1: Various Structural Properties of Catalyst-Underlying-Layer Combinations

Substrate	Underlayer	Catalyst
Silion	N/A	Fe
		Co
	Silicon dioxide (SiO_2)	Fe
		Co
	Titanium (Ti)	Fe
		Co
	Tungstun (W)	Fe
		Co
	Selectively growth CNTs w/o underlayer	Fe

4.1 Influence of catalyst layer thickness

It is known that CNTs grown by low temperature CVD procedures requires a transition metal catalyst [43], and numerous studies have reported the use of Ni, Fe, Co. [55–57]. In this study, the CNTs are grown on silicon p-type (100) substrates. A thin catalyst film (Fe, Co) is deposited on substrates by DC magnetron sputtering. Table 4.2 and 4.3 show that

the relationship between sputtering time and metal catalysts (Fe, Co) thickness, separately. From the experimental results, for both Fe and Co catalysts, CNTs can by synthesized well onto the plain silicon substrates by depositing the thickness around 7nm-12nm. However, once the catalyst films are thicker than 15nm, CNTs are not found at any substrate, instead of graphite. The catalyst thinkess was measured by profilometer.

Table 4.2: Iron catalyst vs. sputtering time

Sputtering time	1min	3min	5min	8min	10min	15min
Iron thickness	t $\leq$ 7nm			$\approx 7nm$	$\approx 10nm$	$\approx 15nm$

Table 4.3: Cobalt catalyst vs. sputtering time

Sputtering time	15sec	30sec	45sec	1min	>1min
Cobalt thickness	t $\leq$ 7nm		$\approx 15nm$	$\approx 25nm$	>25nm

4.2 Influence of underlying layer

CNTs are grown ever different underlying layers of SiO_2, Ti and W. We investigated the Fe and Co catalysts and various underlayers in their respective effectivenss. For using Fe catalyst, the results indicates that nanotubes are grown well on plain Si and SiO_2 underlayer at a certain growth condition. On the other hand, using the Ti or W as underlayer, the high-quality nanotubes cannot be form. For Co catalyst, nanotubes can be only grown on SiO_2 underlayers. The Ti, W and plain silicon are not found nanotubes formation. For plain silicon, the reason could be the formation of silicide, $CoSi_x$ during the high temperature processing [58] . As a result, a barrier layer such as SiO_2 is useful to prevent silicide formation when using Co as catalyst.

4.3 Influence of the deposition temperature

In this study, nanotubes were synthesized at two different deposition temperatures while keeping all other parameters constant. For Fe catalyst, our experimental results indicate

when temperature is below 700 °C, it may not be sufficient for nucleating nanotubes. The temperature may be too low to decompose C_2H_2, hindering growth. Furthermore, the low temperature also limits the graphitization, which increases the condensation of *a*-C [59]. The nanotubes grown at 700 °C are uniform and dense in size. Nevertheless, when the deposition temperature is increased to about 900 °C, the nanotubes are not grown. For Co catalyst, it is found that the nanotubes cannot be grown at 700 °C. However, while increasing the deposition temperature to 850 °C, the nanotubes are successfully grown. According to *C.H. Lin et al.* [60], it is believed that the effect of the substrate temperature is to minimize the thermal energy to activate catalysts to precipitate carbon atoms to form nanotubes.

4.4 Fowler-Nordheim curves

In section 2.4, the field emission properteis of CNTs has been introduced. During the field emission process, when the injected electrons pass through the surface of the CNTs and are emitted into the vacuum towards the anode from the CNTs, the local electric field is enhanced due to the sharp needle like emitting structures of the CNTs compared to the flat structures. According to Fowler-Nordheim (F-N) theory [61], the dependence of the emission current, *I(A)* on the work function ϕ(eV) of the emitting surface and the local electric field just above the emitter surface, $F{=}\beta E{=}\beta V/d$ (V/μm), is exponential, and described by the F-N equation written as:

$$I{=}\frac{k_1\beta^2E^2s}{\phi}\exp\left(-\frac{k_2\phi^{\frac{3}{2}}}{\beta}\right)$$

where s is the emitter area (cm^2) and β is the enhancement factor, determined by the geometric shape of the emitter. The constants $k_1 = 1.54{\times}10^{-6}$(A-eV/$V^2$) and $k_2 = 6.83{\times}10^7$ (eV$^{-3/2}$-V/cm) are given in the literature [62]. In general, the plot of $\ln(1/E^2)$ vs $1/E$ yields a straight line and the slope of the line is proportional to the field enhancement factor, β of the emitters and the intercept gives the emitter area.

4.5 Scanning electron microscope image

In this section, the scanning electron microscope (SEM) images of CNTs samples with different growth conditions and underlying layers are presented. The following SEM images show that the samples with 1 and 5 of iron sputtering time on SiO_2 and 15, 30sec and 1min of cobalt sputtering time on SiO_2. The sample with 5 min iron and 8 min graphite sputtering time can yield very good-quality MWNTs on both plain silicon and SiO_2, as shown in Figure 4.3. Figure 4.5 and 4.6 were used cobalt as catlayst to deposit CNTs. Using cobalt to synthesize CNTs, they are obviously shorter than using Fe as catalyst under the same growth time. Figure 4.7 shows that when catalyst thickness is too thick, then carbon cluster will be formed instead of CNTs. The cross-sectional SEM image of vertically-aligned and randomly-oriented MWCNTs is shown as Figure 4.8 and Figure 4.9, separately. Figure. 4.10 is the patterned CNTs of SEM image.

4.5.1 SEM images of CNTs with different catalysts sputtering time and underlayers

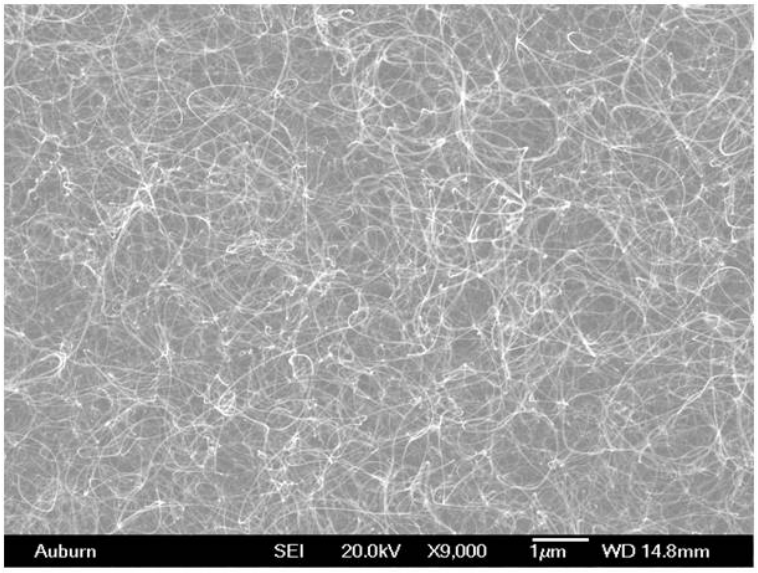

Figure 4.1: 1min Fe sputtering time on SiO_2 underlayer

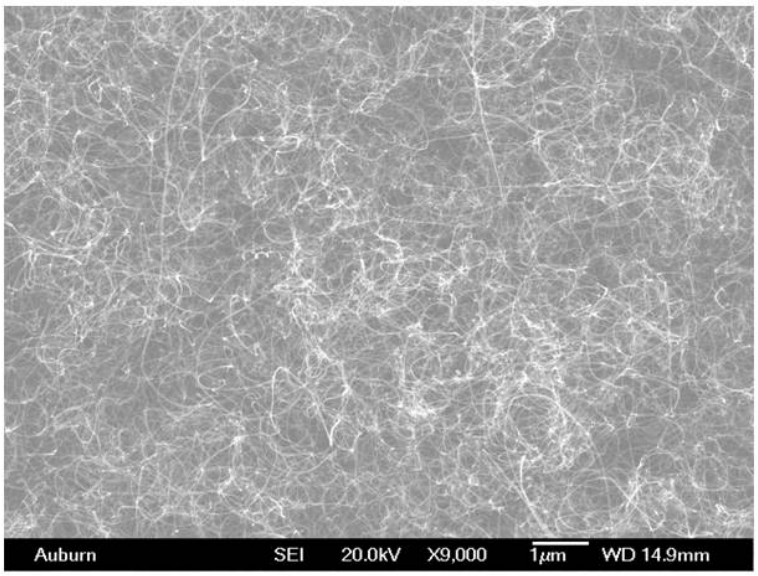

Figure 4.2: 5min Fe sputtering time on SiO_2 underlayer

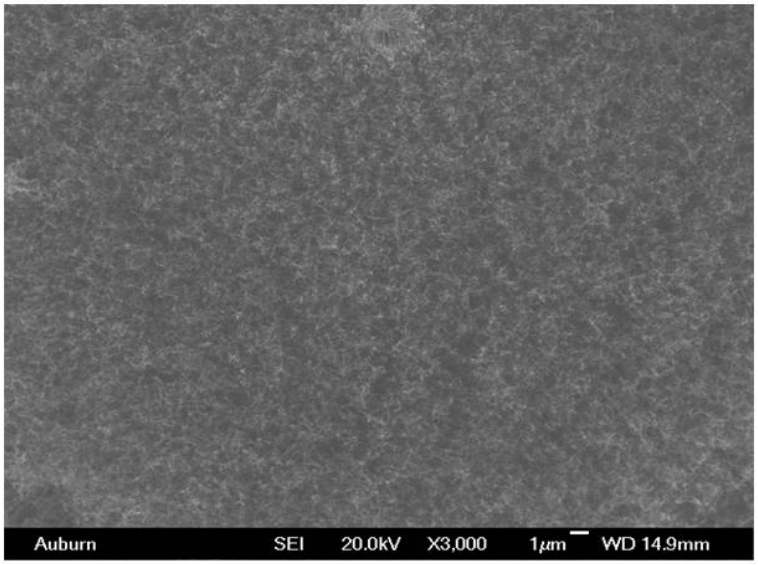

Figure 4.3: 5min Fe with Carbon 8 min sputtering time on SiO_2 underlayer

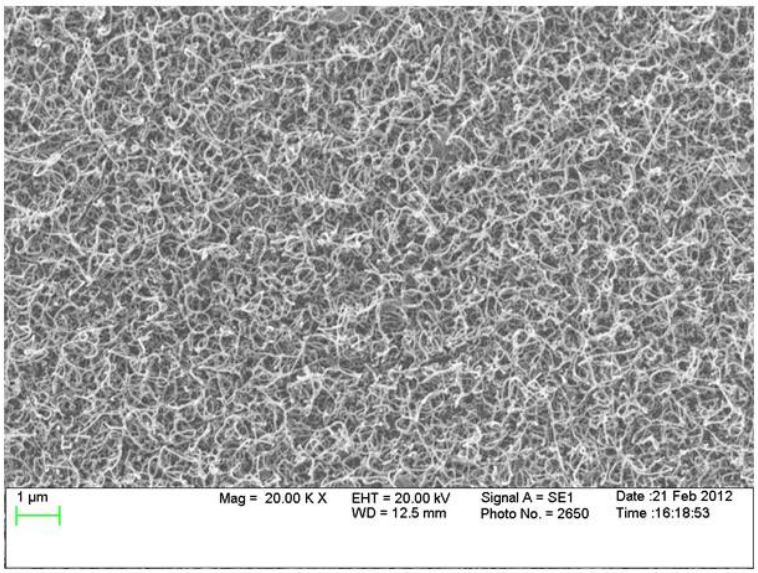

Figure 4.4: 5min Fe sputtering time on SiO_2 underlayer

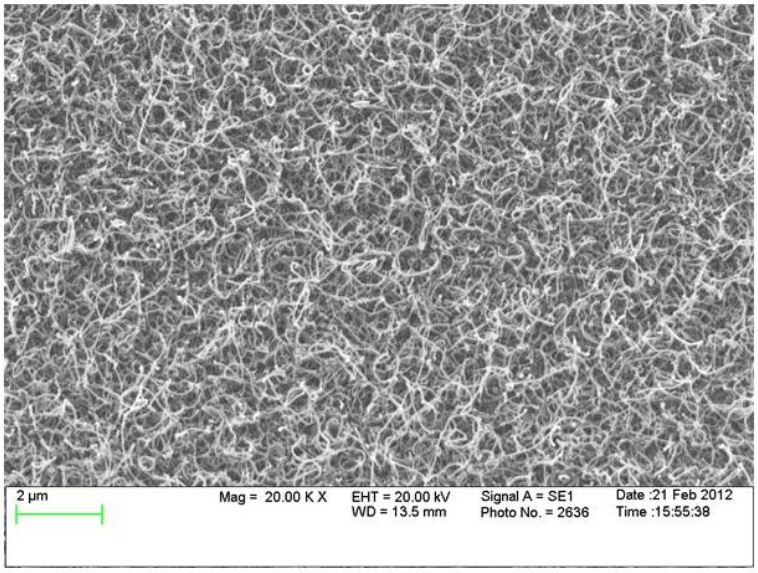

Figure 4.5: 15 sec Cobalt sputtering time on SiO_2 underlayer

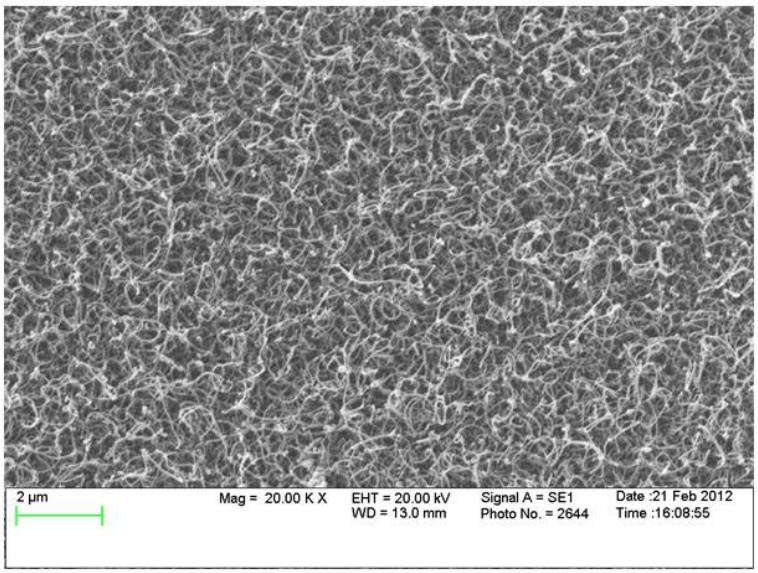

Figure 4.6: 30 sec Cobalt sputtering time on SiO_2 underlayer

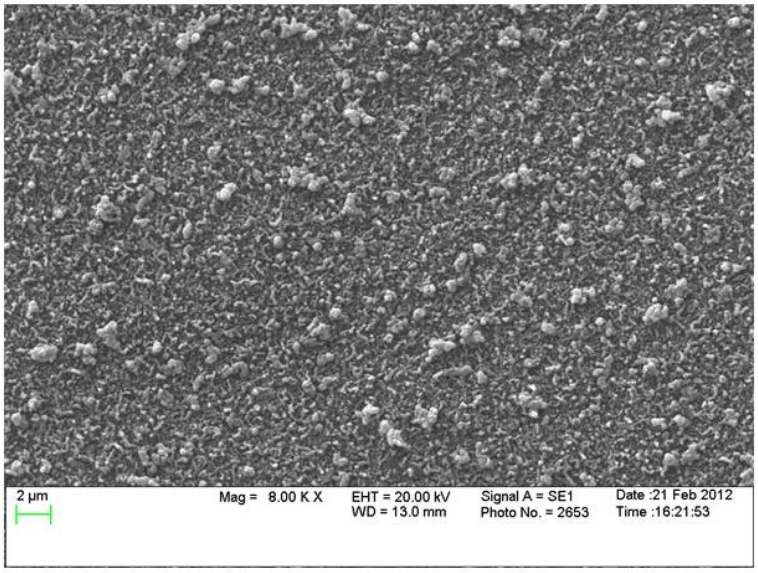

Figure 4.7: Cobalt sputtering time above 1min on SiO_2 underlayer

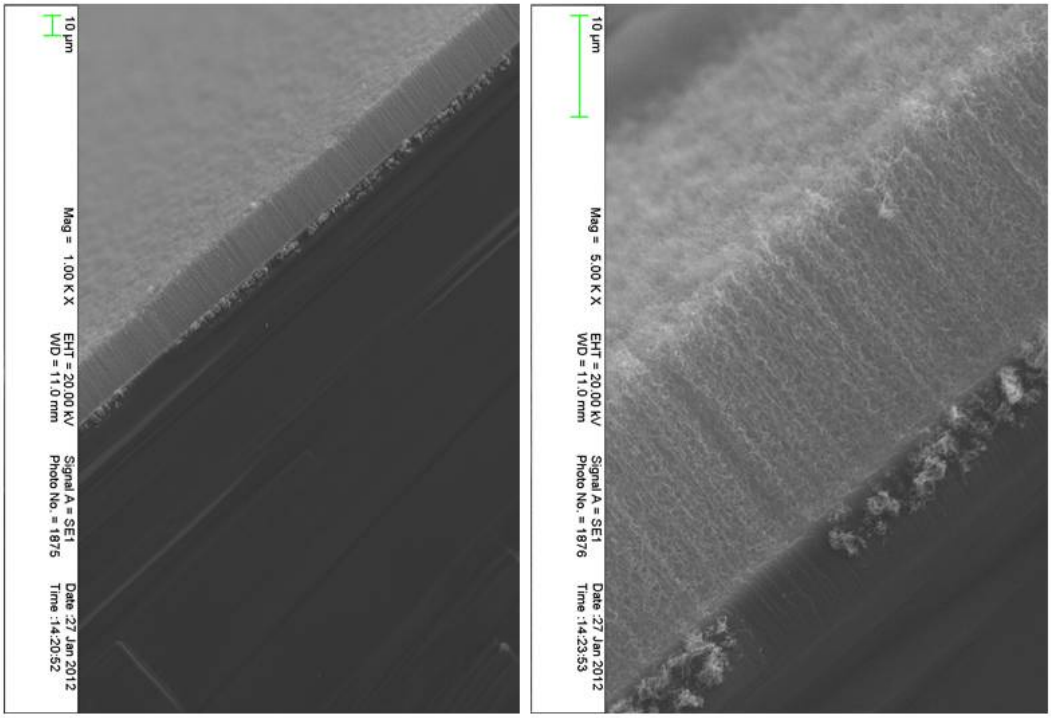

Figure 4.8: SEM image of vertically-aligned multi-wall carbon nanotubes (VA-MWCNTs).

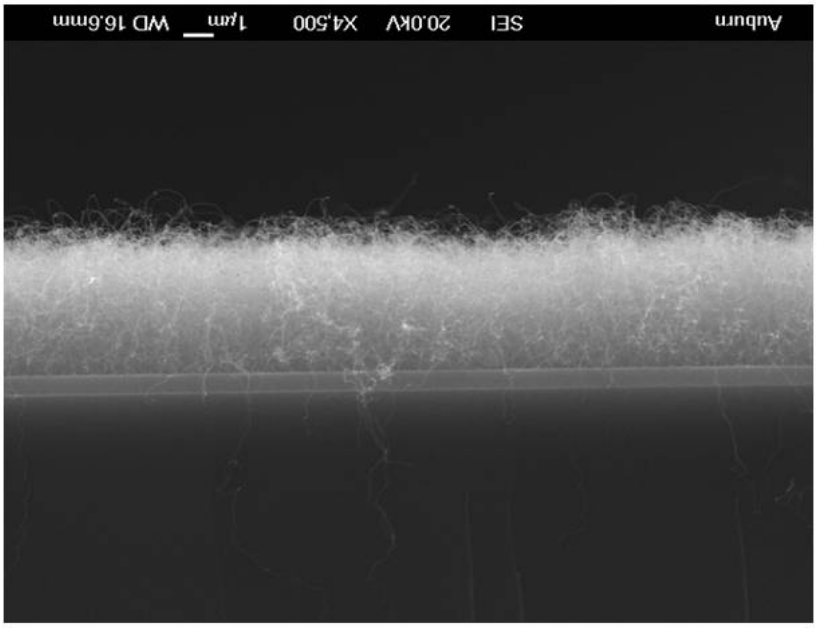

Figure 4.9: Cross-sectional SEM image of randomly-oriented MWCNTs.

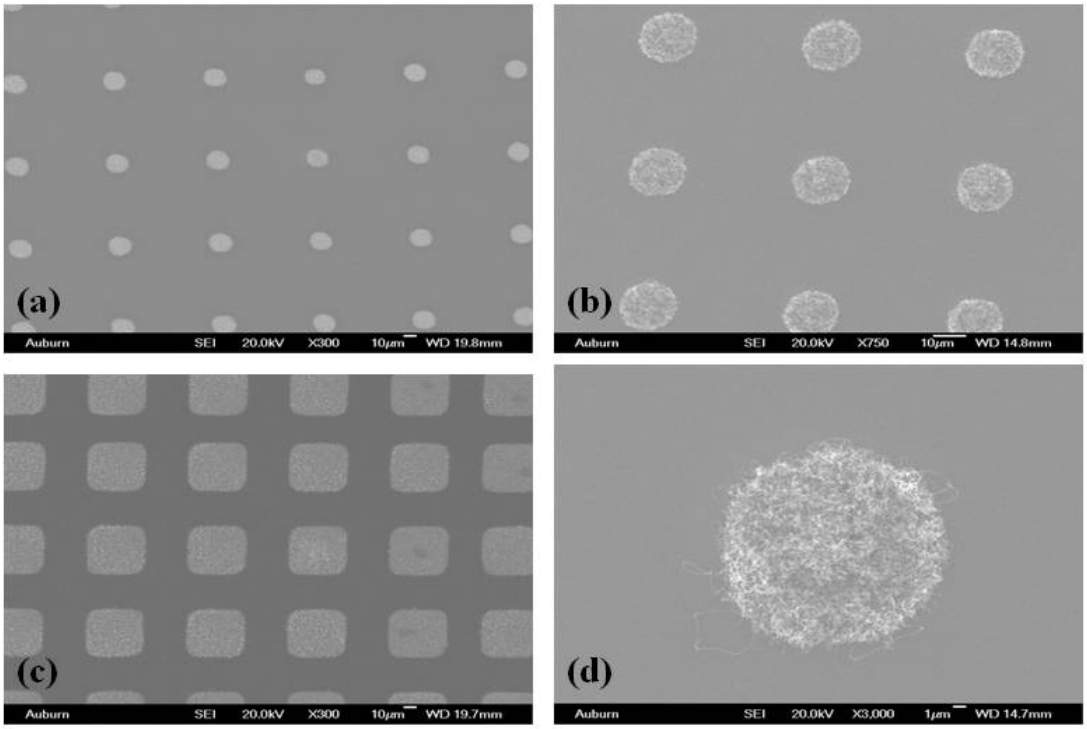

Figure 4.10: SEM image of patterned CNTs array (a) 25μm circle array with 25μm spacing, (b) 25μm diameter circle array with 50μm spacing, (c) 50μm $\times$ 50μm square array with 25μm spacing, (d) a close-up image of a single CNT bundle (from a circle array sample)

Table 4.4: Various Structural Properties of Catalyst-Underlying-Layer Combinations

Specimen Label	**Substrate**	**Underlying Layer**	**Catalyst Type (XX)**	**Pre-treatment[a] (YY)**	**Types of CNTs**	**Growth Condition[c]**	**Note[b]**
S01-XX-YY[d]	Silicon[e]	Oxide($0.6\mu m$)	Iron[f]	N/A	Random	T: 700 °C; t:20min	Table4.5
				w/ depositing graphite	Vertically-Aligned	Ar:C_2H_2=75:25sccm	
			Cobalt[g]	N/A	Random	T: 850 °C[h]; t:20min	Table4.6
				w/ depositing graphite	Random	Ar:C_2H_2=75:25sccm	
S02-XX-YY	Silicon	N/A[i]	Iron	N/A	Random	T: 700 °C; t:20min	Table4.7
				w/ depositing graphite	Vertically-Aligned	Ar:C_2H_2=75:25sccm	
			Cobalt	N/A	Random	T: 850 °C; t:20min	Table4.8
				w/ depositing graphite	Random	Ar:C_2H_2=75:25sccm	
S03-XX-YY	Silicon	Titanium($0.6\mu m$)[j]	Iron	N/A	Random	T: 700 °C; t:20min	Table4.9
				w/ depositing graphite	Random	Ar:C_2H_2=75:25sccm	
			Cobalt	N/A	Random	T: 850 °C; t:20min	Table4.10
				w/ depositing graphite	Random	Ar:C_2H_2=75:25sccm	
S04-XX-YY	Silicon	Tungsten($0.4\mu m$)[k]	Iron	N/A	N/A	T: 700 °C; t:20min	Table4.11
				w/ depositing graphite	N/A	Ar:C_2H_2=75:25sccm	
			Cobalt	N/A	N/A	T: 850 °C; t:20min	Table4.12
				w/ depositing graphite	N/A	Ar:C_2H_2=75:25sccm	

[a] Specimen with depositing graphite were then annealed in air at 300 °C for 8hrs [63]
[b] For detailed information, refer to the table
[c] The grwoth time of specimens all are 20min in a gas mixture of Argon and Acetylene(75:25sccm) in the pressure 70Torr
[f] The iron purity is 99.99%
[d] XX: the deposition time of catalyst, YY: the deposition time of graphite
[e] Use n-type $< 100 >$ Si wafer, resistivity 1 to 5 Ω-cm
[g] The cobalt purity is 99.99%
[h] It is believed that substrate temperature is to minimize the thermal energy to activate catalysts to form nanotubes [60]
[i] RCA cleaning process(a short immersion in a 1:50 solution of HF + H2O) to remove native oxide layer
[j] The titanium purity is 99.99%
[k] The tungsten purity is 99.99%

Table 4.5: Various Structural Properties of Catalyst-Underlying-Layer Combinations

Specimen Label	**Substrate**	**Underlying Layer**	**Catalyst Type (XX)**	**Pre-treatment (YY)**	**Types of CNTs**	**Growth Condition**[a]	**Note**[b]
S05-XX-YY[c]	Silicon	N/A	Iron	N/A	Random	T: 700 °C; t:20min Ar:C_2H_2=75:25sccm	Table4.13

[b]For detailed information, refer to the table
[a]The grwoth time of specimens all are 20min in a gas mixture of Argon and Acetylene(75:25sccm) in the pressure 70Torr
[c]Selective grwon CNTs

Table 4.6: MWNTs growth on the catalyst-coated(Fe) substrate w/ SiO2 underlayer

Specimen Label	**Thickness of Catalyst**	**SEM Image**	**Type of CNTs**	**Field Emission Characteristics**
S01-Fe-1min-00	$t \leq$ 7nm	Low density growth	Random	Turn on field $\approx 1.86V/\mu m$ Saturation curent $\approx 5.4 \times 10^{-3} A/cm^2$
S01-Fe-3min-00		Low density growth	Random	Turn on field $\approx 1.57V/\mu m$ Saturation curent $\approx 5.2 \times 10^{-3} A/cm^2$
S01-Fe-5min-00		High density growth	Random	Turn on field $\approx 1.71V/\mu m$ Saturation curent $\approx 4.1 \times 10^{-3} A/cm^2$
S01-Fe-8min-00	$t \approx$ 7nm	High density growth	Random	Turn on field $\approx 1.71V/\mu m$ Saturation curent $\approx 4.8 \times 10^{-3} A/cm^2$
S01-Fe-10min-00	$t \approx$ 10nm	High density growth	Random	Turn on field $\approx 1.57V/\mu m$ Saturation curent $\approx 4.9 \times 10^{-3} A/cm^2$
S01-Fe-15min-00	$t \approx$ 15nm	No growth[a]	N/A	N/A
S01-Fe-5min-C-1min	Fe catalyst: $t \leq$ 7nm [a]	High density growth	Random	Turn on field $\approx 1.71V/\mu m$ Saturation curent $\approx 4.1 \times 10^{-3}$
S01-Fe-5min-C-3min		High density growth	Random	Turn on field $\approx 1.71V/\mu m$ Saturation curent $\approx 5.3 \times 10^{-3} A/cm^2$
S01-Fe-5min-C-5min		High density growth	Random	Turn on field $\approx 1.71V/\mu m$ Saturation curent $\approx 4.78 \times 10^{-3} A/cm^2$
S01-Fe-5min-C-8min		Extreme density growth	Vertically Aligned	Turn on field $\approx 2.14V/\mu m$ Saturation curent $\approx 1.78 \times 10^{-3} A/cm^2$
S01-Fe-5min-C-10min		High density growth	Random	Turn on field $\approx 1.57v/\mu m$ Saturation curent $\approx 4.58 \times 10^{-3} A/cm^2$
S01-Fe-5min-C-15min		No growth	N/A	N/A

[a]Form the carbon cluster

[a]Choosing Fe-5min as the base,and then pretreated by depositing graphite(C) and annealing 8hrs.

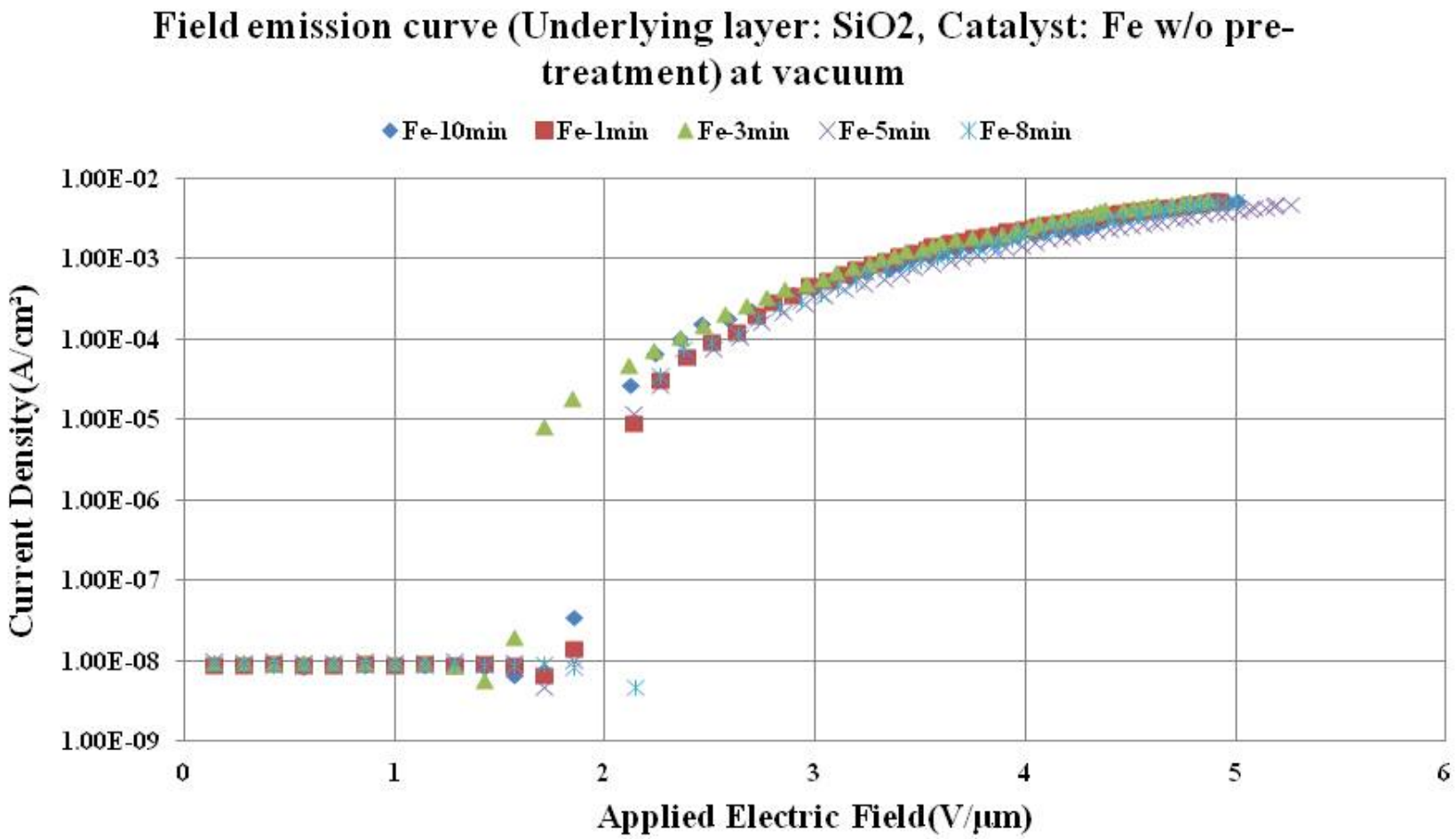

Figure 4.11: Field emission curve for growing CNTs on SiO_2 using Fe as catalyst w/o pre-treatment

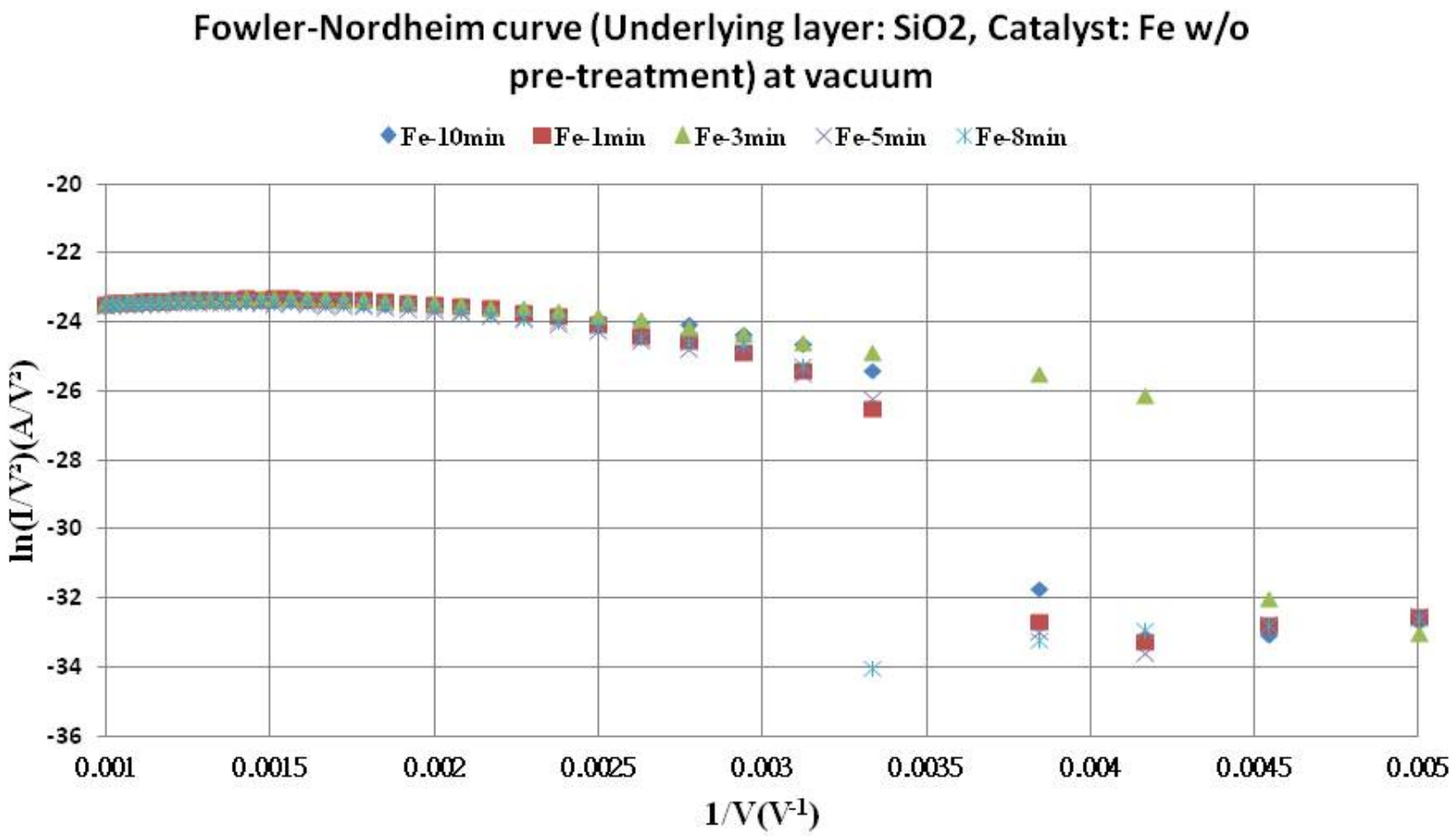

Figure 4.12: Fowler-Nordeim curve of CNT grown on SiO_2 using Fe as catalyst w/o pre-treatment

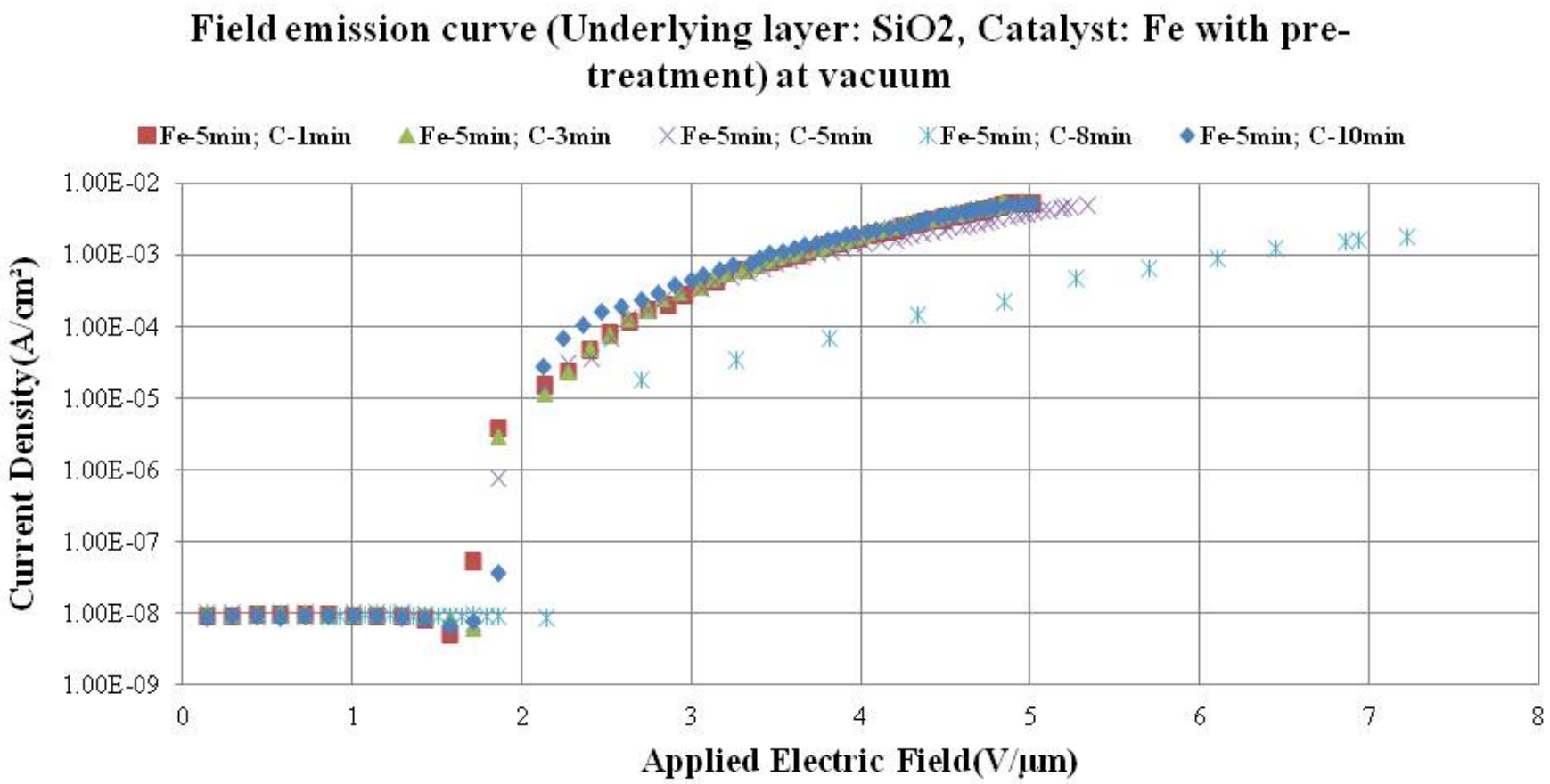

Figure 4.13: Field emission curve for growing CNTs on SiO_2 using Fe as catalyst with pre-treatment

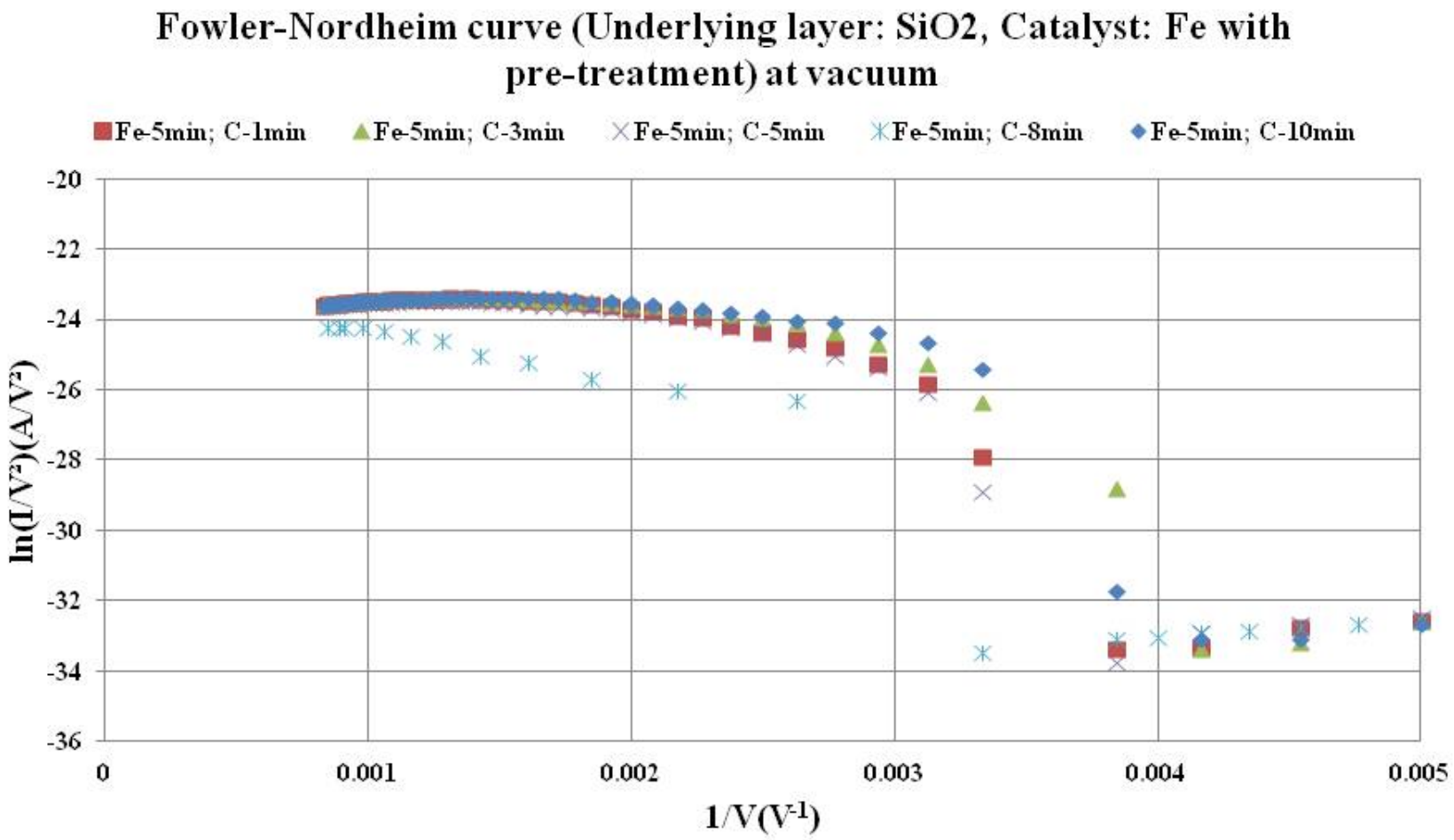

Figure 4.14: Fowler-Nordeim curve of CNT grown on SiO_2 using Fe as catalyst with pre-treatment

Table 4.7: MWNTs growth on the catalyst-coated(Co) substrate w/ SiO2 underlayer

Specimen Label	**Thickness of Catalyst**	**SEM Image**	**Type of CNTs**	**Field Emission Characteristics**
S01-Co-15sec-00	$t \leq 7$nm	Low density growth	Random	Turn on field $\approx 2.72V/\mu m$ Saturation curent $\approx 4.5 \times 10^{-3} A/cm^2$
S01-Co-30sec-00		Low density growth	Random	Turn on field $\approx 5.57V/\mu m$ Saturation curent $\approx 2.09 \times 10^{-3} A/cm^2$
S01-Co-45sec-00	$t \approx 15$nm	Low density growth	Random	Turn on field $\approx 1.72V/\mu m$ Saturation curent $\approx 3.8 \times 10^{-3} A/cm^2$
S01-Co-1min-00	$t \approx 25$nm	Low density growth	Random	Turn on field $\approx 2.72V/\mu m$ Saturation curent $\approx 3.7 \times 10^{-3} A/cm^2$
S01-Co-Above 1min-00	$t > 25$nm	No growth	N/A	N/A
S01-Co-45sec-C-3min	Co catalyst: $t \approx 25$nm	No growth	N/A	N/A
S01-Co-45sec-C-4min		No growth	N/A	N/A
S01-Co-45sec-C-5min		No growth	N/A	N/A
S01-Co-45sec-C-7min		No growth	N/A	N/A
S01-Co-45sec-C-10min		No growth	N/A	N/A

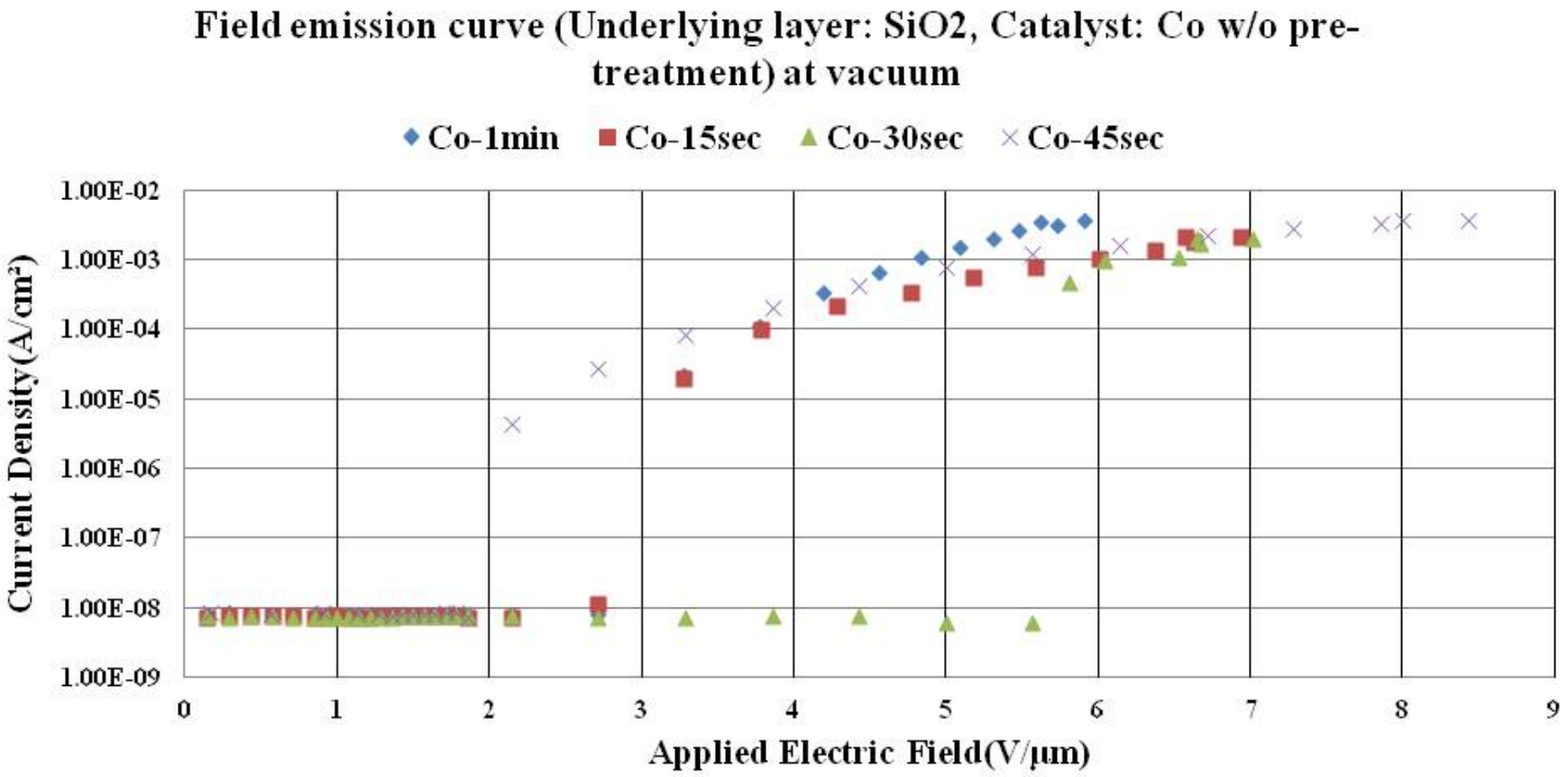

Figure 4.15: Field emission curve for growing CNTs on SiO_2 using Co as catalyst w/o pre-treatment

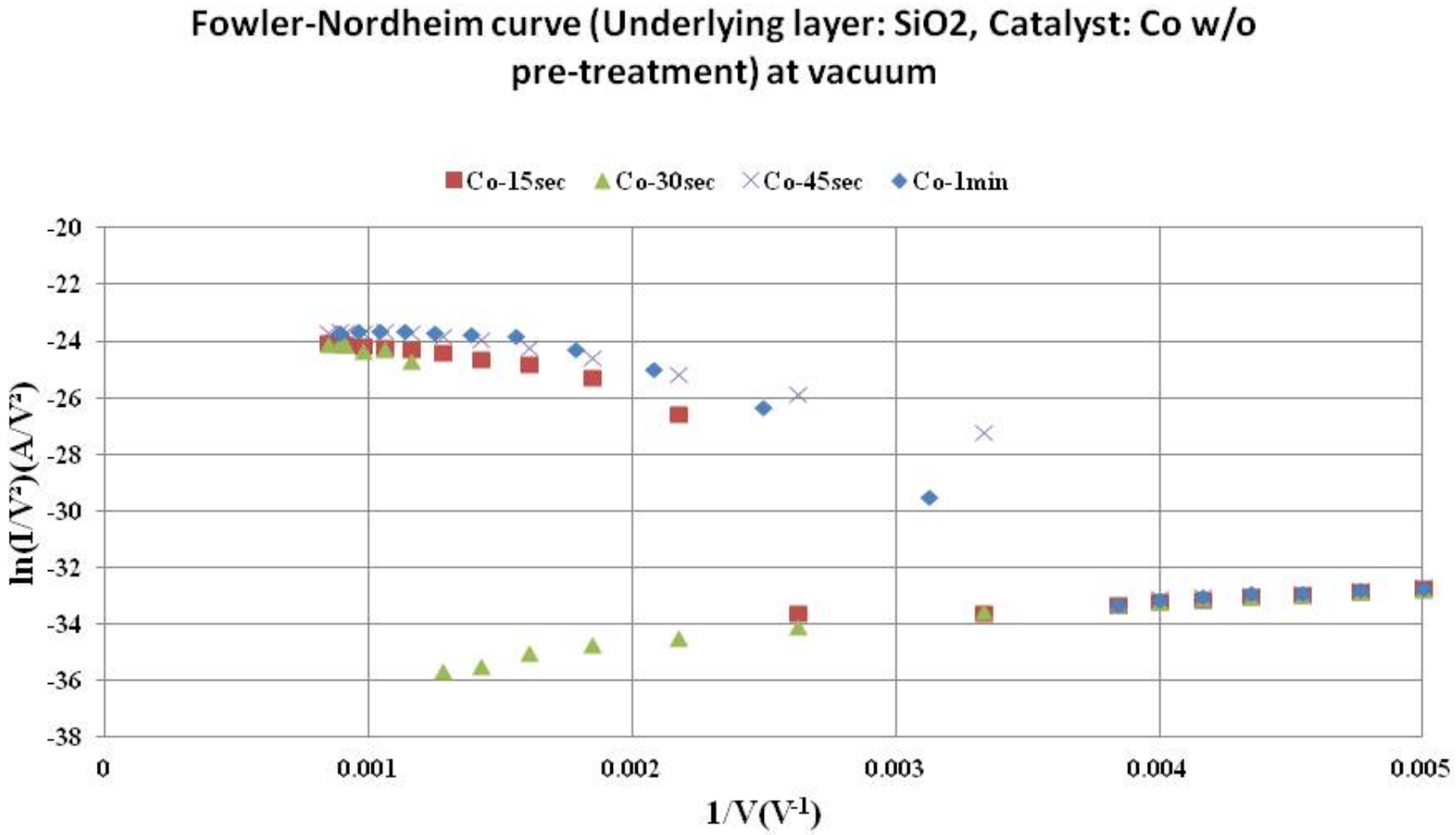

Figure 4.16: Fowler-Nordeim curve of CNT grown on SiO_2 using Co as catalyst w/o pre-treatment

Table 4.8: MWNTs growth on the catalyst-coated(Fe) substrate w/o SiO2 underlayer

Specimen Label	**Thickness of Catalyst**	**SEM Image**	**Type of CNTs**	**Field Emission Characteristics**
S02-Fe-1min-00	$t \leq$ 7nm	Low density growth	Random	Turn on field $\approx 1.21V/\mu m$ Saturation curent $\approx 4.33 \times 10^{-3}A/cm^2$
S02-Fe-3min-00		Low density growth	Random	Turn on field $\approx 1.22V/\mu m$ Saturation curent $\approx 6.47 \times 10^{-3}A/cm^2$
S02-Fe-5min-00		High density growth	Random	Turn on field $\approx 1.78V/\mu m$ Saturation curent $\approx 5.45 \times 10^{-3}A/cm^2$
S02-Fe-8min-00	$t \approx$ 7nm	High density growth	Random	Turn on field $\approx 1.43V/\mu m$ Saturation curent $\approx 6.4 \times 10^{-3}A/cm^2$
S02-Fe-10min-00	$t \approx$ 10nm	High density growth	Random	Turn on field $\approx 1.14V/\mu m$ Saturation curent $\approx 6.6 \times 10^{-3}A/cm^2$
S02-Fe-15min-00	$t \approx$ 15nm	No growth[a]	N/A	N/A
S02-Fe-5min-C-1min	Fe catalyst: $t \leq$ 7nm [a]	High density growth	Random	Turn on field $\approx 1.14V/\mu m$ Saturation curent $\approx 5.74 \times 10^{-3}A/cm^2$
S02-Fe-5min-C-3min		High density growth	Random	Turn on field $\approx 1.37V/\mu m$ Saturation curent $\approx 5.1 \times 10^{-3}A/cm^2$
S02-Fe-5min-C-5min		High density growth	Random	Turn on field $\approx 1.36V/\mu m$ Saturation curent $\approx 6.4 \times 10^{-3}A/cm^2$
S02-Fe-5min-C-8min		Extreme density growth	Vertically Aligned	Turn on field $\approx 2.14V/\mu m$ Saturation curent $\approx 1.41 \times 10^{-4}A/cm^2$
S02-Fe-5min-C-10min		High density growth	Random	Turn on field $\approx 1.86v/\mu m$ Saturation curent $\approx 2.08 \times 10^{-3}A/cm^2$
S02-Fe-5min-C-15min		No growth	N/A	N/A

[a]Form the carbon cluster

[a]Choosing Fe-5min as the base,and then pretreated by depositing graphite(C) and annealing 8hrs.

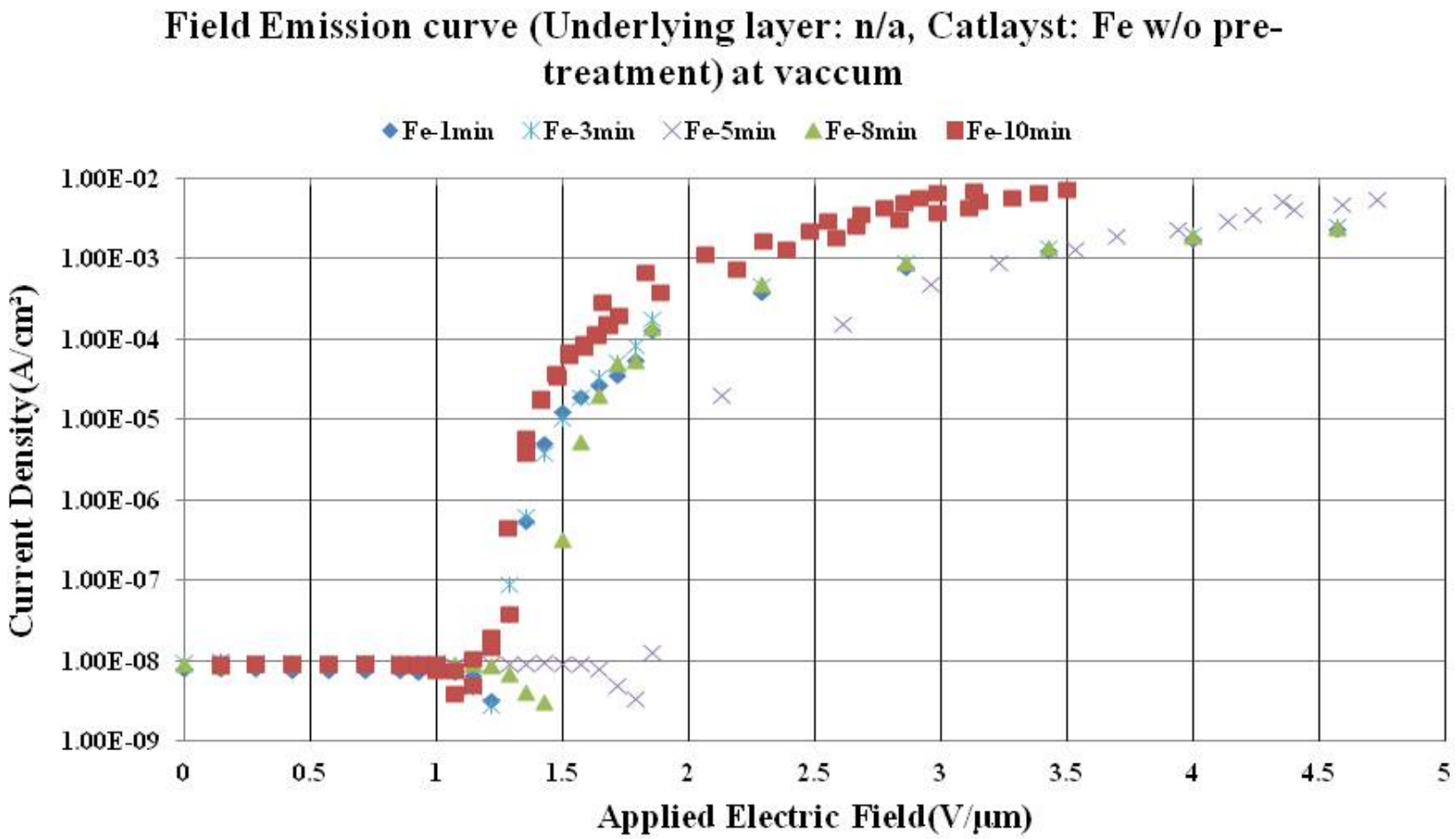

Figure 4.17: Field emission curve for growing CNTs on plain silicon using Fe as catalyst w/o pre-treatment

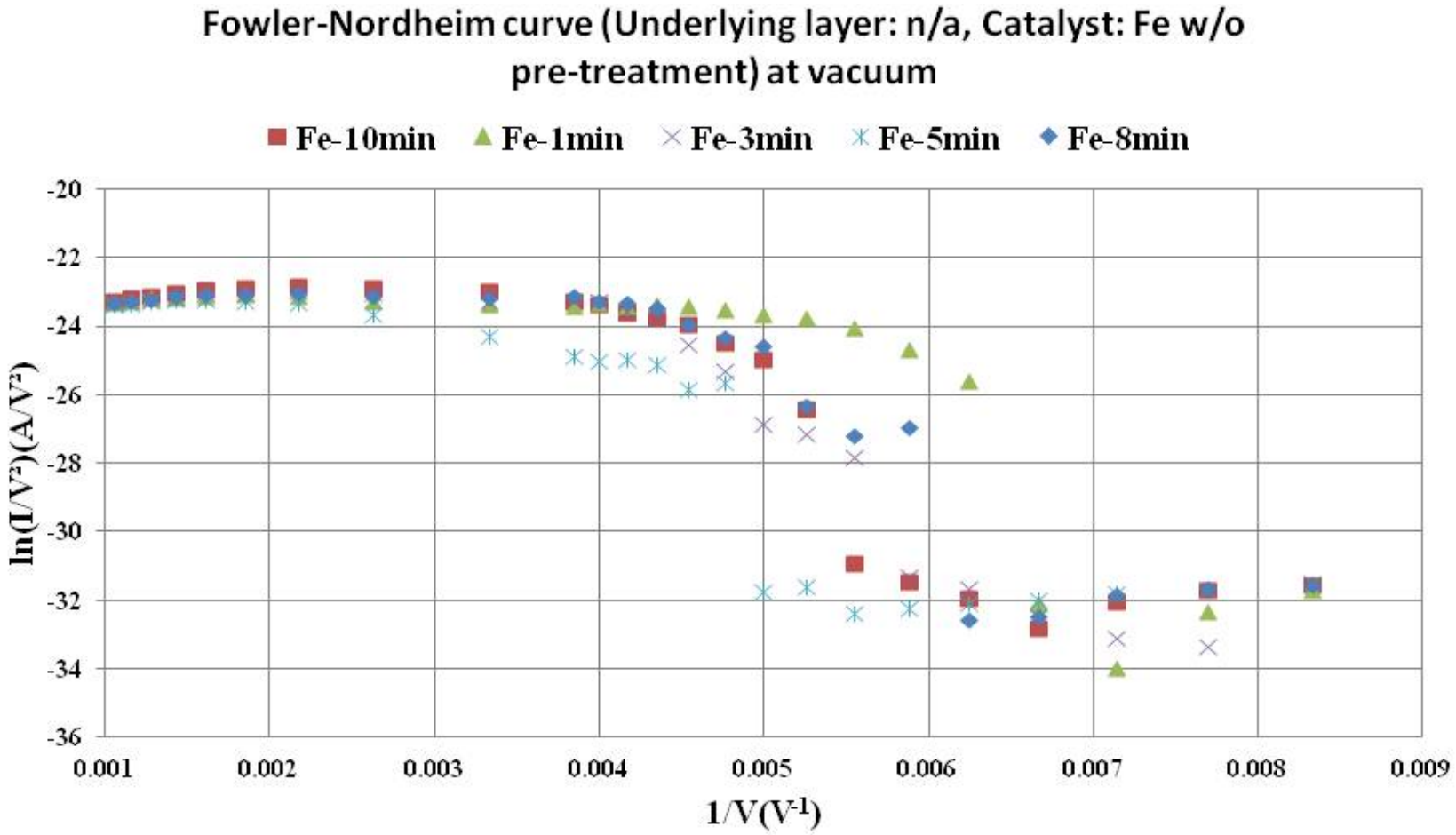

Figure 4.18: Fowler-Nordeim curve of CNT grown on plain silicon using Fe as catalyst w/o pre-treatment

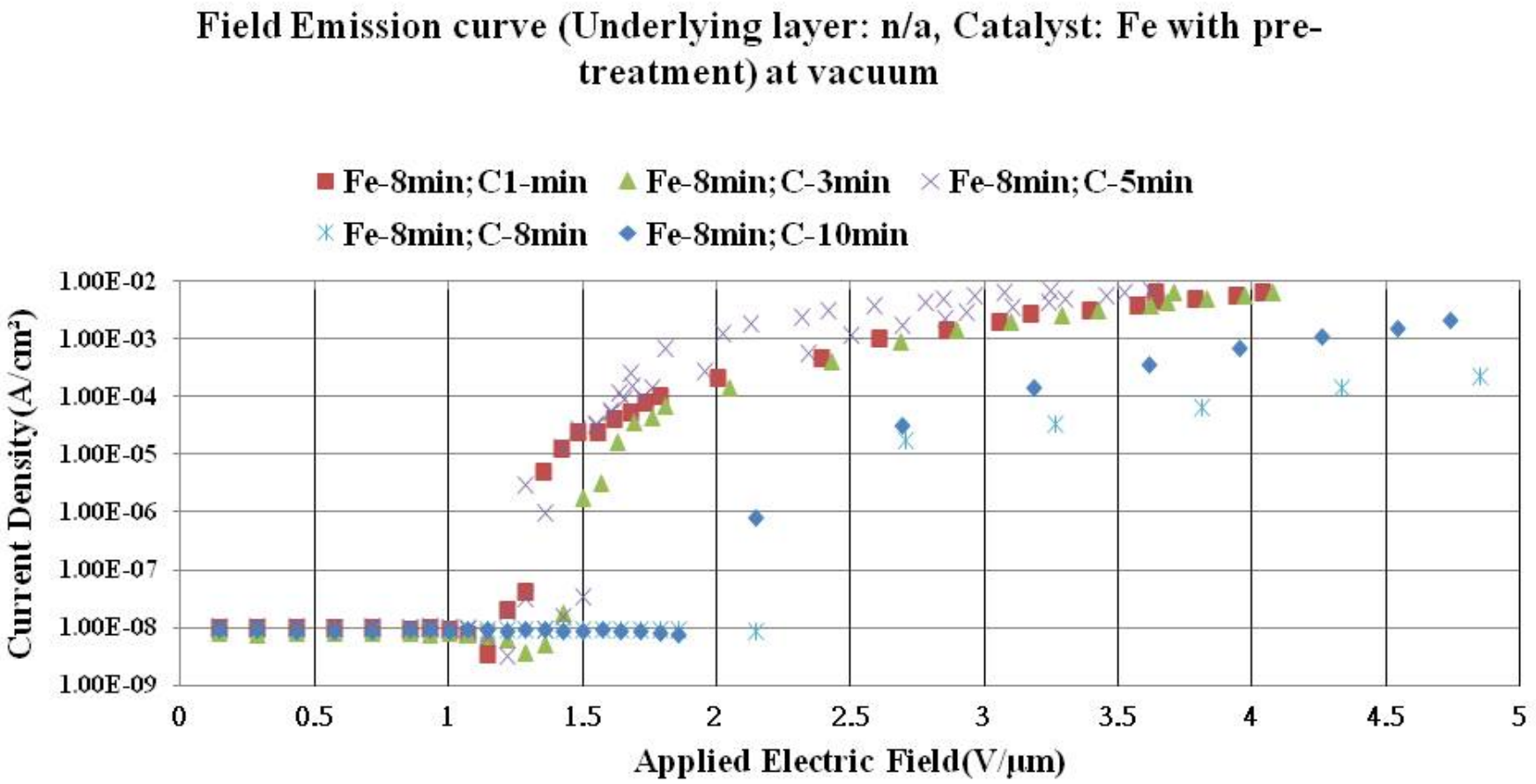

Figure 4.19: Field emission curve for growing CNTs on plain silicon using Fe as catalyst with pre-treatment

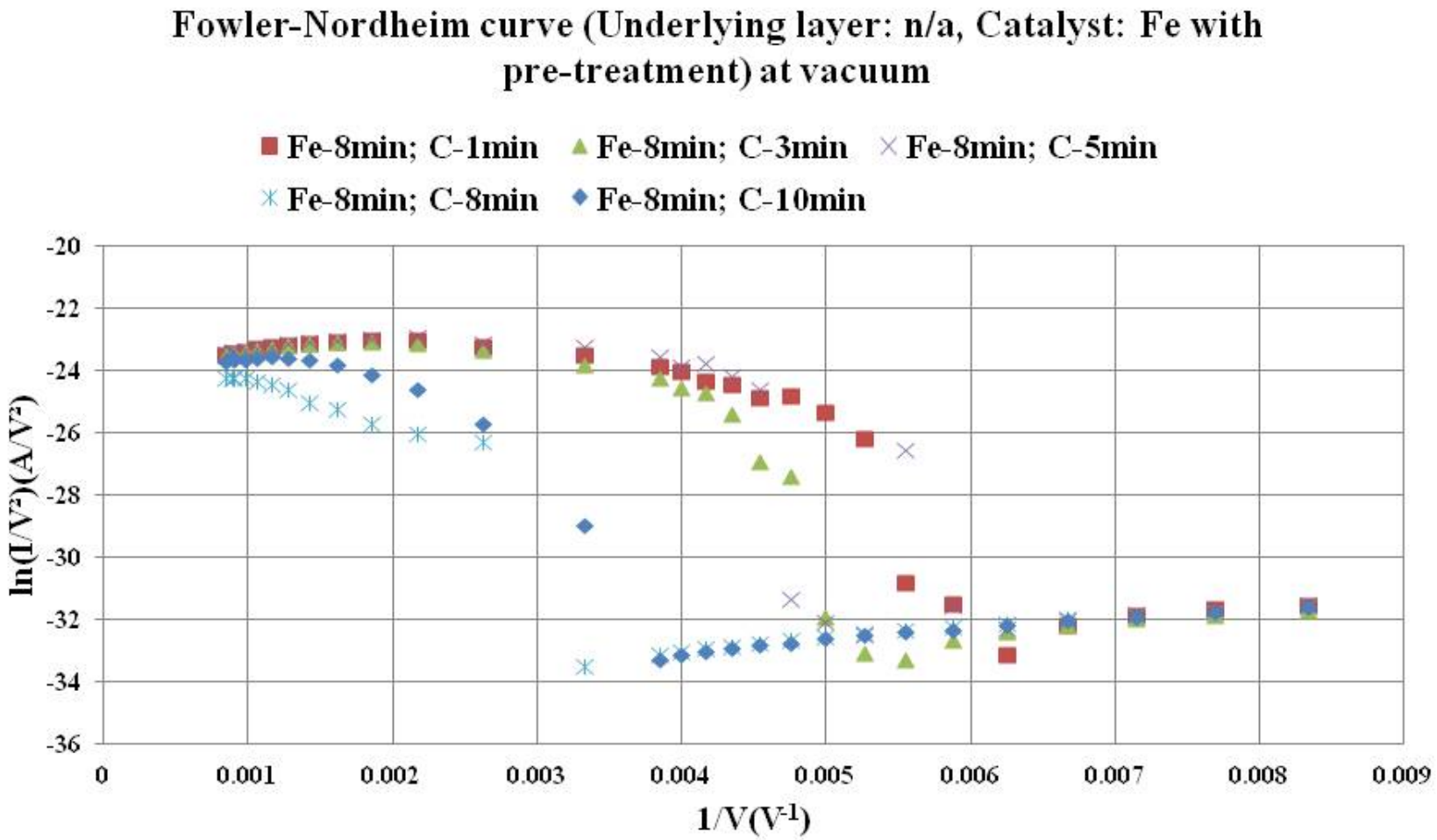

Figure 4.20: Fowler-Nordeim curve of CNT grown on plain silicon using Fe as catalyst with pre-treatment

Table 4.9: MWNTs growth on the catalyst-coated(Co) substrate w/o SiO2 underlayer

Specimen Label	**Thickness of Catalyst**	**SEM Image**	**Type of CNTs**	**Field Emission Characteristics**
S02-Co-15sec-00	$t \leq 7$nm	No growth	N/A	N/A
S02-Co-30sec-00		No growth	N/A	N/A
S02-Co-45sec-00	$t \approx 15$nm	No growth	N/A	N/A
S02-Co-1min-00	$t \approx 25$nm	No growth	N/A	N/A
S02-Co-45sec-C-3min	Co catalyst: $t \approx 25$nm	No growth	N/A	N/A
S02-Co-45sec-C-4min		No growth	N/A	N/A
S02-Co-45sec-C-5min		No growth	N/A	N/A
S02-Co-45sec-C-7min		No growth	N/A	N/A
S02-Co-45sec-C-10min		No growth	N/A	N/A

Table 4.10: MWNTs growth on the catalyst(Fe)-underlying Ti layer-coated substrate

Specimen Label	**Thickness of Catalyst**	**SEM Image**	**Type of CNTs**	**Field Emission Characteristics**
S03-Fe-5min-00	Fe catalyst: $t \leq 7$nm Ti layer $\approx 0.6\mu m$	Very low density growth	Random	Turn on field $\approx 2.9V/\mu m$ Saturation curent $\approx 2.52 \times 10^{-3} mA/cm^2$
S03-Fe-8min-00		Very low density growth	Random	Turn on field $\approx 3.2V/\mu m$ Saturation curent $\approx 1.54 \times 10^{-3} mA/cm^2$
S03-Fe-10min-00		Very low density growth	Random	Turn on field $\approx 2.3V/\mu m$ Saturation curent $\approx 2.64 \times 10^{-3} mA/cm^2$
S03-Fe-5min-C-5min	Fe catalyst: $t \leq 7$nm	Very low density growth	Random	Turn on field $\approx 2.14V/\mu m$ Saturation curent $\approx 2.04 \times 10^{-3} mA/cm^2$
S03-Fe-5min-C-8min		Very low density growth	Random	Turn on field $\approx 2.71V/\mu m$ Saturation curent $\approx 1.43 \times 10^{-3} mA/cm^2$
S03-Fe-5min-C-10min		Very low density growth	Random	Turn on field $\approx 3.86V/\mu m$ Saturation curent $\approx 1.55 \times 10^{-3} mA/cm^2$

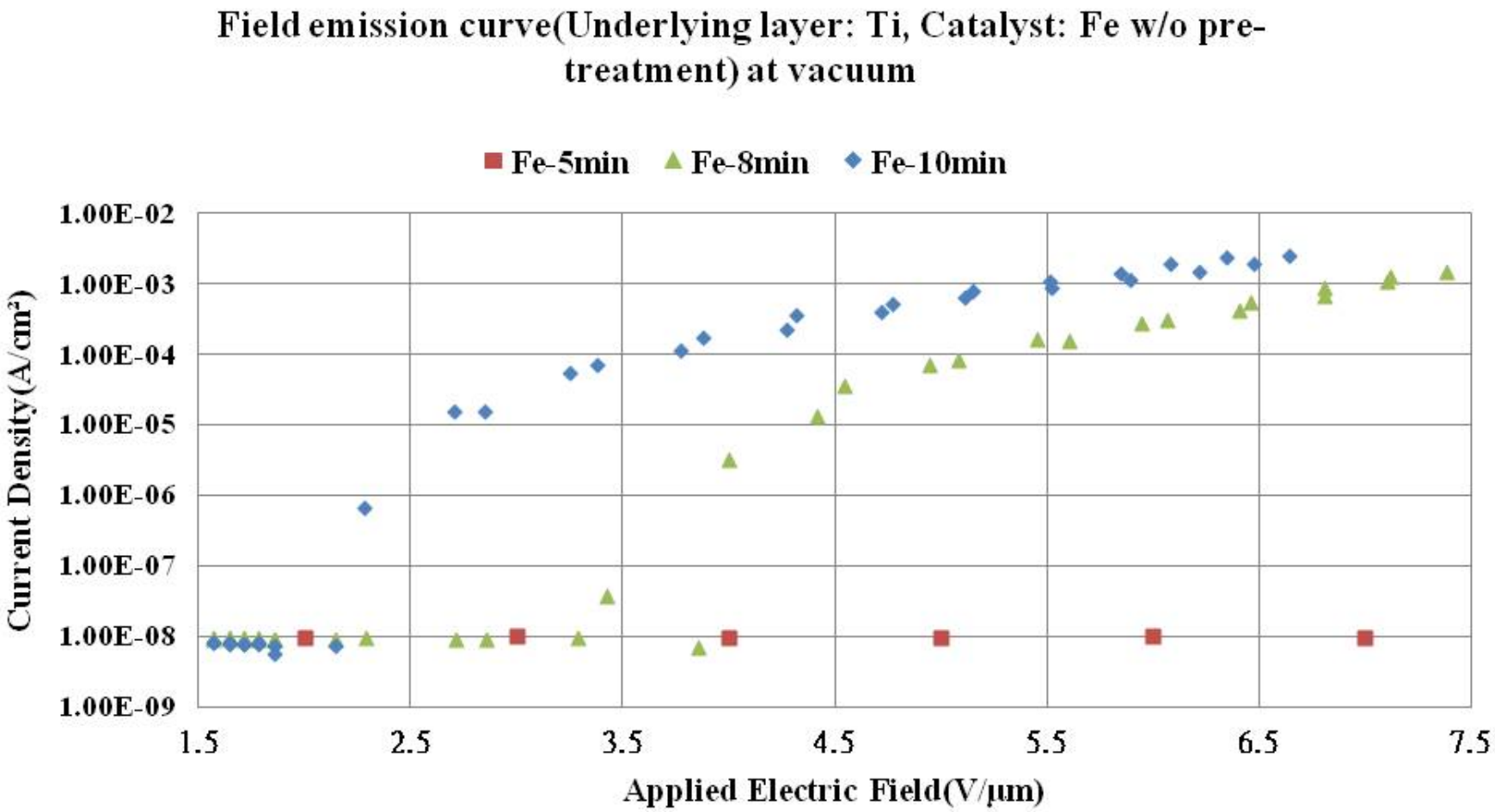

Figure 4.21: Field emission curve for growing CNTs on Ti underlying layer using Fe as catalyst w/o pre-treatment

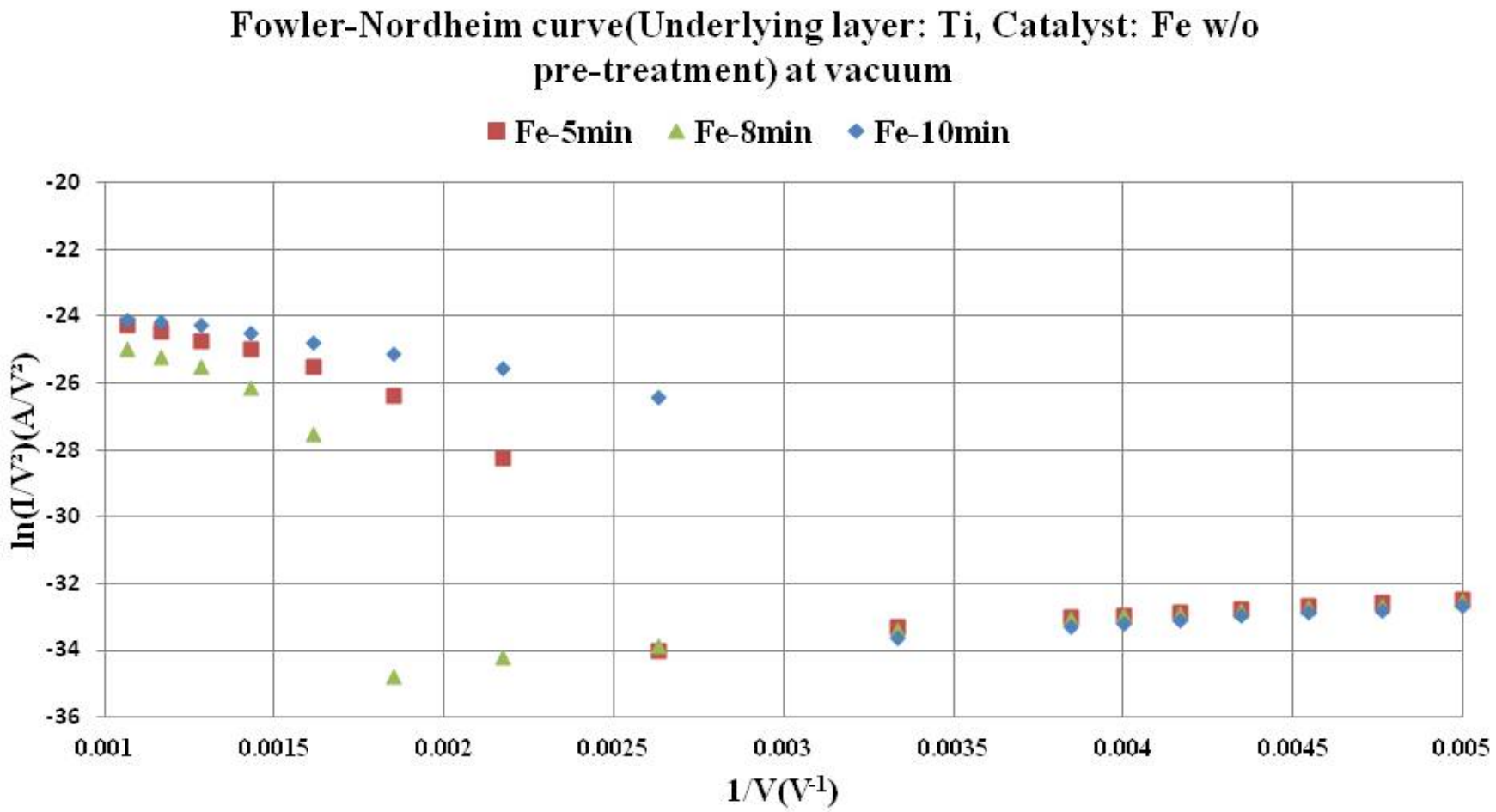

Figure 4.22: Fowler-Nordeim curve of CNT grown on plain silicon using Fe as catalyst w/o pre-treatment

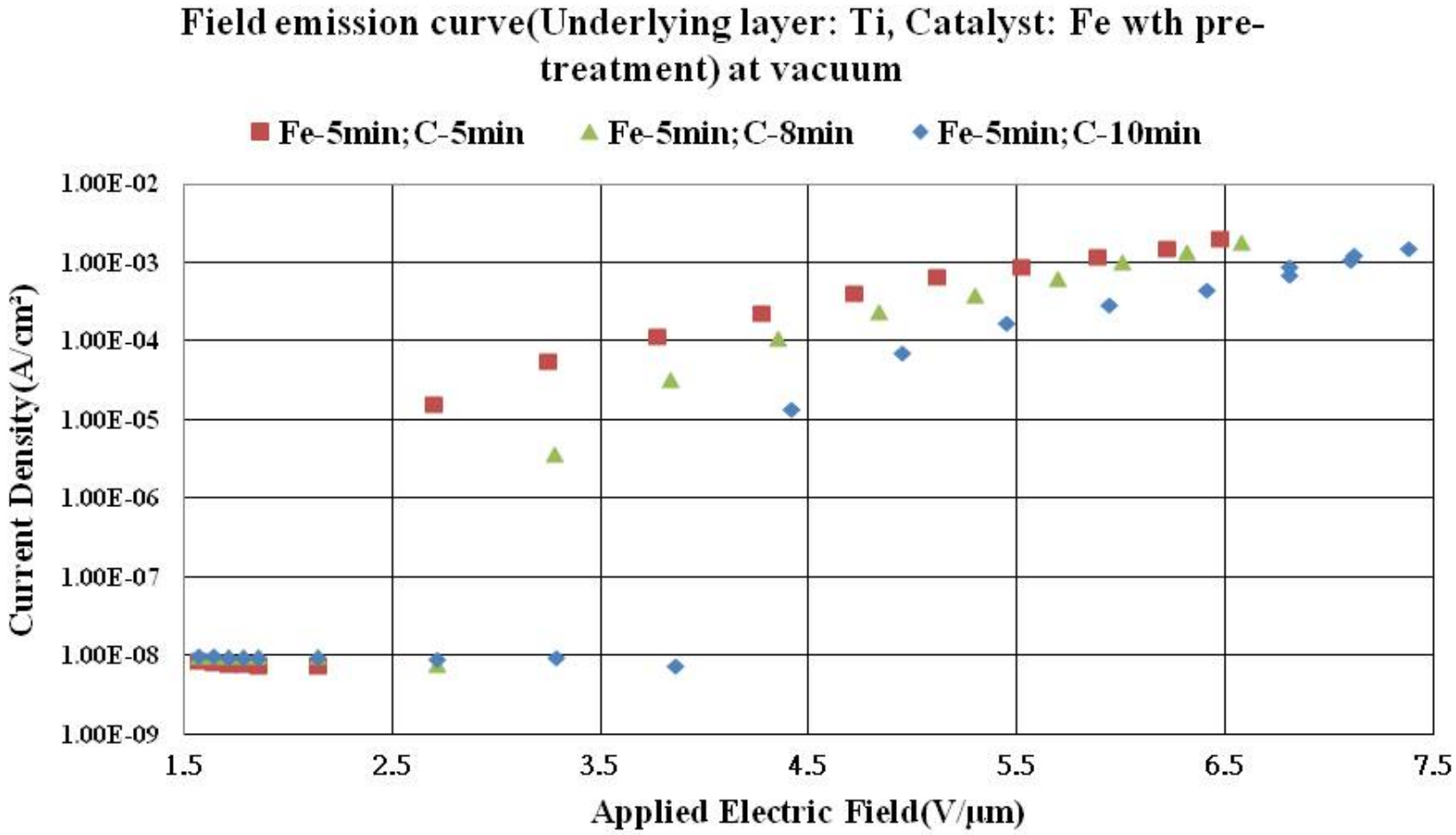

Figure 4.23: Field emission curve for growing CNTs on Ti underlying layer using Fe as catalyst with pre-treatment

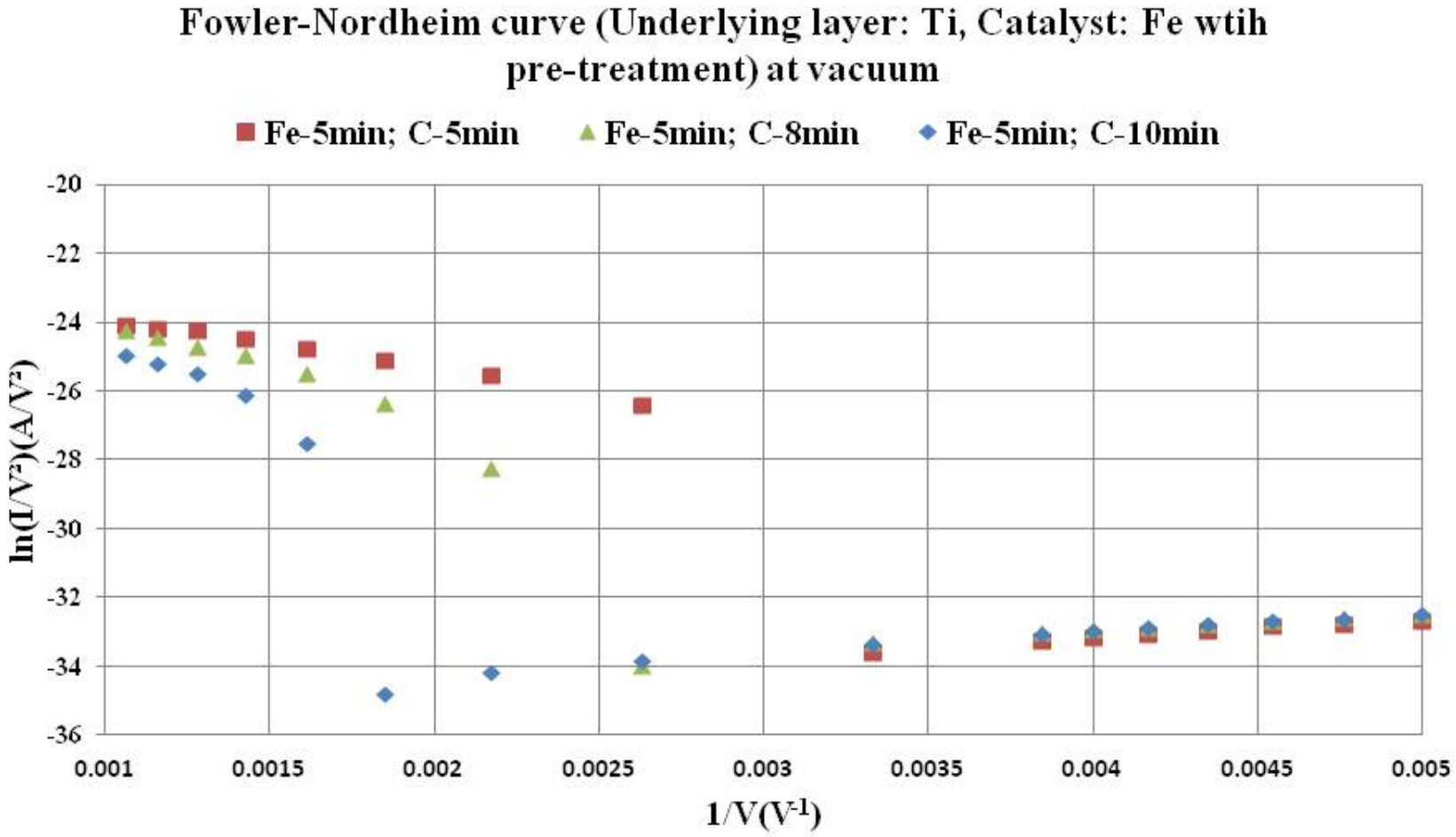

Figure 4.24: Fowler-Nordeim curve of CNT grown on Ti underlying layer using Fe as catalyst with pre-treatment

Table 4.11: MWNTs growth on the catalyst(Co)-underlying Ti layer-coated substrate

Specimen Label	**Thickness of Catalyst**	**SEM Image**	**Type of CNTs**	**Field Emission Characteristics**
S03-Co-30sec-00	$t \leq 7$nm	No growth	N/A	N/A
S03-Co-45sec-00	$t \approx 15$nm	No growth	N/A	N/A
S03-Co-1min-00	$t \approx 25$nm	No growth	N/A	N/A
S03-Co-1min-C-5min	$t \approx 25$nm	No growth	N/A	N/A
S03-Co-1min-C-8min		No growth	N/A	N/A
S03-Co-1min-C-10min		No growth	N/A	N/A

Table 4.12: MWNTs growth on the catalyst(Fe)-underlying W layer-coated substrate

Specimen Label	**Thickness of Catalyst**	**SEM Image**	**Type of CNTs**	**Field Emission Characteristics**
S04-Fe-5min-00	$t \leq$ 7nm	No growth	N/A	N/A
S04-Fe-8min-00	$t \approx$ 7nm	No growth	N/A	N/A
S04-Fe-10min-00	$t \approx$ 10nm	No growth	N/A	N/A
S04-Fe-5min-C-5min	Fe catalyst: $t \leq$ 7nm	No growth	N/A	N/A
S04-Fe-5min-C-8min		No growth	N/A	N/A
S04-Fe-5min-C-10min		No growth	N/A	N/A

Table 4.13: MWNTs growth on the catalyst(Co)-underlying W layer-coated substrate

Specimen Label	**Thickness of Catalyst**	**SEM Image**	**Type of CNTs**	**Field Emission Characteristics**
S04-Co-30sec-00	$t \leq 7$nm	No growth	N/A	N/A
S04-Co-45sec-00	$t \approx 15$nm	No growth	N/A	N/A
S04-Co-1min-00	$t \approx 25$nm	No growth	N/A	N/A
S04-Co-1min-C-5min	Co catalyst: $t \approx 25$nm	No growth	N/A	N/A
S04-Co-1min-C-8min		No growth	N/A	N/A
S04-Co-1min-C-10min		No growth	N/A	N/A

Table 4.14: Selective growth of MWNTs on the catalyst(Fe)-coated substrate w/o SiO2

Sample Label	**Size**	**Shape**	**Array Spacing**	**SEM Image**	**Type of CNTs**	**Field Emission Characteristics**
S05-Fe-5min-00	$25\mu m$ in diameter	Circle	$25\mu m$	High density	Random	Turn on field $\approx 2.26V/\mu m$ Saturation curent $\approx 2.47 \times 10^{-3}A/cm^2$
	$25\mu m$ in diameter	Circle	$50\mu m$	High density	Random	Turn on field $\approx 3.12V/\mu m$ Saturation curent $\approx 0.3 \times 10^{-3}A/cm^2$
	$25\mu m$ in diameter	Circle	$100\mu m$	High density	Random	Turn on field $\approx 2.42V/\mu m$ Saturation curent $\approx 1 \times 10^{-3}A/cm^2$
	$50\mu m \times 50\mu m$	Square	$25\mu m$	High density	Random	Turn on field $\approx 2.28V/\mu m$ Saturation curent $\approx 4 \times 10^{-3}A/cm^2$
	0.5cm × 0.5cm	Square	0.5cm	High density	Random	Turn on field $\approx 2.82V/\mu m$ Saturation curent $\approx 0.4 \times 10^{-4}A/cm^2$

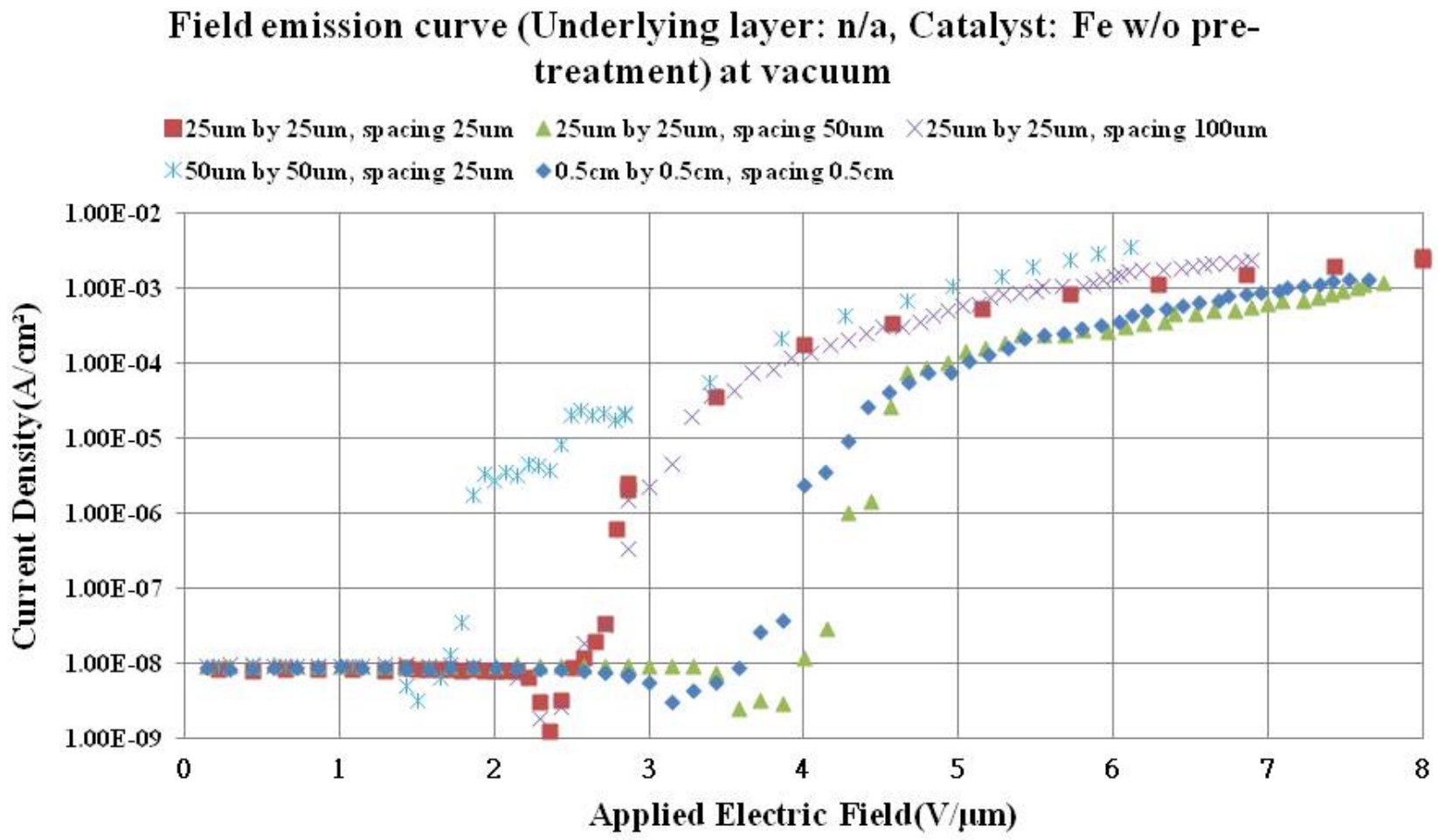

Figure 4.25: Field emission curve for growing selective CNTs on plain silicon using Fe as catalyst w/o pre-treatment

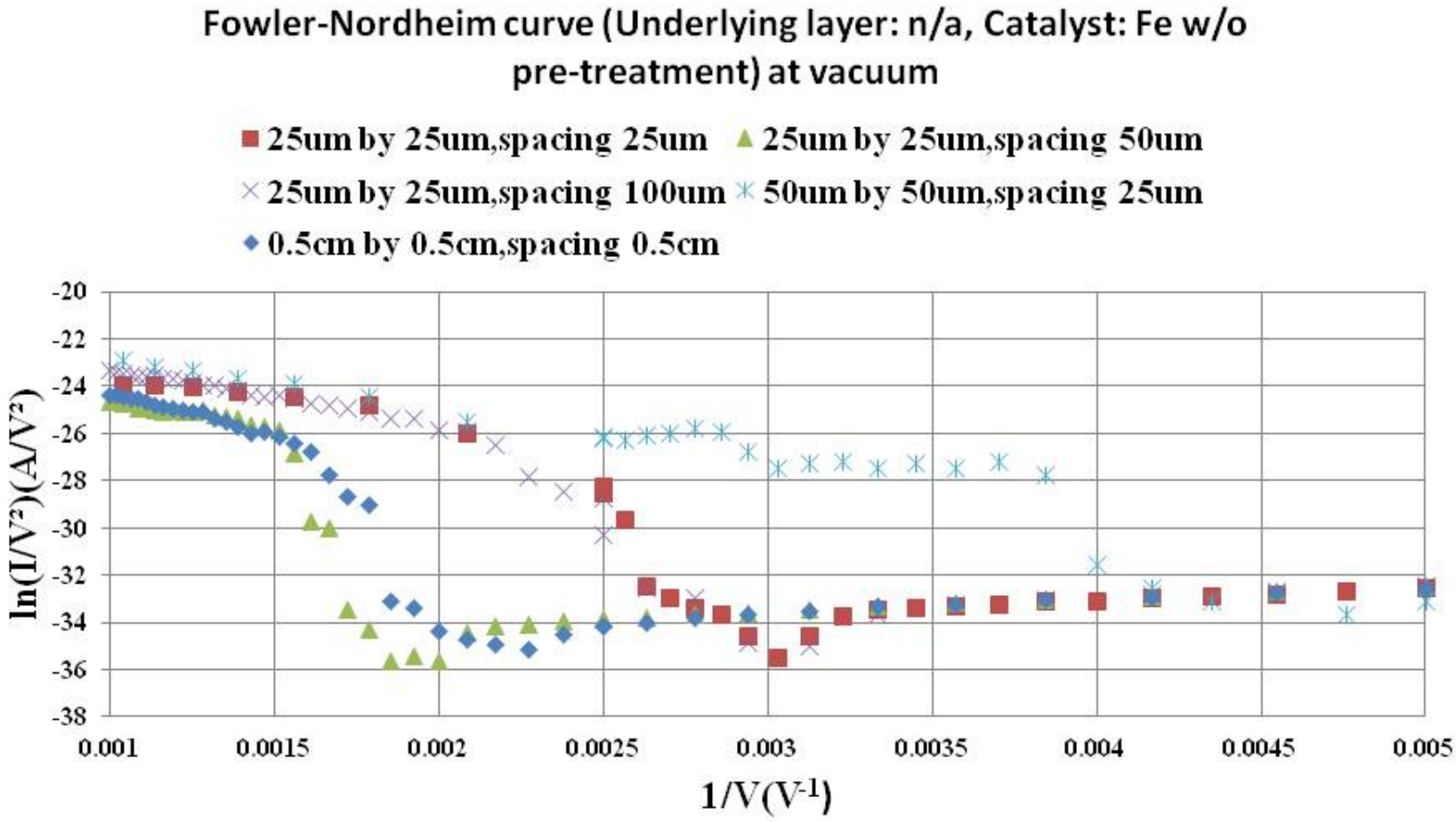

Figure 4.26: Fowler-Nordeim curve of selective CNT grown on plain silicon using Fe as catalyst w/o pre-treatment

Chapter 5

SUMMARY AND FUTURE DIRECTIONS

Since the discovery of carbon nanotubes (CNTs), many studies have been carried out on their synthesis. With their outstanding electrical, structure, and physical properties, CNTs are envisioned to impact furture electronic applications such as nanoelectronics, sensors, electrodes, and nanophotonics. These applications generally require controlled growth on patterned substrates. Therefore, there has been a strong focus on using thermal chemical vapor deposition (CVD) technique to realized CNT structures for these applications. Field emission is one of the most advanced and broadly studied applications of CNTs. They can emit electrons easily due to their high aspect ratios, compared to other cold-cathode materials.

In this work, CNTs have been selective and non-selective grown on a variety of catalyst-coated underlaying layers (plain silicon, SiO_2, Ti, W) substrate at two different temperatures (700 °C, 800 °C) by using thermal chemical vapor technique. We investigated their field emission characteristics. From the experiemtal results, it clearly indicates that metal catlayst thickness is a critical parameter for the growth of CNTs. In addition, the deposition temperature and underlayers also play the important roles. Field emission results from carbon nanotube showed clearly the Fowler-Nordheim behavior. Vertically-aligned CNTs can be successfully synthesized at a certain growth condition. There are many still obstacle remaining. The growth conditions of CNTs have not been fully determined such as gas flow rate (acetylene, argon), deposition temperature, pressure, catalyst thickness, underlying layer, etc. The field emisision and underlayers mechanism for CNTs growth need to be deeply investigated.

Bibliography

[1] S. Iijima. Helical microtubules of graphitic carbon. *Nature*, 354:56–58, November 1991.

[2] A. A. Talin, K. A. Dean, and J. E. Kaskie. *Solid-State Electron*, 45:963, 2001.

[3] J. M. Bonard, H. Kind, T. Stockli, and L. Nilsson. *Solid-State Electron*, 45:893, 2001.

[4] H. Murakami, M. Hirakawa, C. Tanaka, and H. Yamakawa. *Appl. Phys. Lette*, 76:1776, 2000.

[5] W. Zhu, C. Bower, G. P. Kochankski, and S. Jin. *Solid-State Electron*, 45:921, 2001.

[6] Ramesh Bokka. Master's thesis, Auburn University, ECE Department, May 2011.

[7] Anastasios John Hart. PhD thesis, Massacusetts Institute of Technology, August 2006.

[8] T. Hayashi, Y.A. Kim, T. Matoba, M. Esaka, K. Nishimura, T. Tsukada, M. Endo, and M.S. Dresselhaus. *Nano Letters*, pages 887–889, 2003.

[9] T. W. Ebbesen, H. Hiura, J. Fujita, Y. Ochiai, S. Matsui, and K. Tangiaki. *Chem. Phys. Lett.*, 209:83–90, 1993.

[10] A. Thess, R. Lee, P. Nikolaev, H. Dai, P. Petit, J. Robert, C. Xu, Y.H. Lee, S.G. Kim, A.G. Rinzler, D.T. Colbert, G.E. Scuseria, D. Tomanek, J.E. Fischer, and R.E. Smalley. *Science*, 273:483, 1996.

[11] C.J. Lee and J. Park. *Appl. Phys. Lett.*, 77:3397, 2000.

[12] Haitao Zhao. PhD thesis, Auburn University, August 2012.

[13] OTTO ZHOU, HIDEO SHIMODA, BO GAO, SOOJIN OH, LES FLEMING, and GUOZHEN YUE. Materials Science of Carbon Nanotubes: Fabrication, Integration, and Properties of Macroscopic Structures of Carbon Nanotubes. *Acc. Chem. Res.*, pages 1045–1053, 2002.

[14] Bhupesh Chandra. PhD thesis, Columbia Uniersity, 2009.

[15] Anton Anisimov. PhD thesis, Aalto University, 2010.

[16] Mauricio Terrones. Science and technology of the twenty-first century: Synthesis, Properties and Applications of Carbon Nanotubes. *Annu. Rev. Mater.Res.*, pages 419–501, 2003.

[17] M. S. Dresselhaus, G. Dresselhaus, and Ph. Avouris. Carbon nanotubes, Topics in Applied Physics. 2001.

[18] M.S. Dresselhaus, G. Dressehaus, and P.C. Eklund. Science of Fullenrenes and Carbon Nanotubes. 1996.

[19] Chao Liu. Cold electron emitters using chemically vapor deposited carbon nanotubes. Master's thesis, Auburn University, ECE Department, 2000.

[20] R. Saito, G. Dresselhaus, and M.S. Dresselhaus. *Appl. Phys.*, 73:494, 1993.

[21] M.S. Dresselhaus, G. Dressehaus, R. Saito, and A. Jorio. Raman spectroscopy of Carbon Nanotubes. *Physics Reports*, 2004.

[22] Ryuichi Kuzuo, Masami Terauchi, and Michiyoshi Tanaka. Electron Energy-Loss Spectra of Carbon Nanotubes. *Japanese Journal of Applied Physics*, 1992.

[23] Mayumi Kosaka, Thomas W. Ebbesen, Hidefumi Hiura, and Katsumi Tanigaki. Electron spin resonance of carbon nanotubes. *Chemical Physcis Letters*, 1994.

[24] L. P. Biro, TS. Lazarescu, Ph. Lambin, P. A. Thiry, A. Fonseca, J. B. Nagy, and A. A. Lucas. Scanning tunneling microscope investigation of carbon nanotubes produced by catalytic decomposition of acetylene. *Physical Review B*, 1997.

[25] T.W. Ebbesen, H. Lezec, H. Hiura, J.W. Bennett, H.F. Ghaemi, and T. Thio. *Nature*, 54:382, 1996.

[26] A. Thess, R. Lee, P. Nikolaev, H. Dai, P. Petit, J. Robert, C. Xu, Y.H. Lee, S.G. Kim, A.G. Rinzler, D.T. Colbert, G.E. Scuseria, D. Tomanek, J.E. Fischer, and R.E. Smalley. *Science*, 273:483, 1994.

[27] O. Lourie abd H.D. Wagner. *Mater. Res.*, 13:9, 1998.

[28] M.F. Yu, B.S. Files, S. Arepalli, and R.S. Ruoff. *Phys. Rev. Lett.*, 84:24, 2000.

[29] C.A. Cooper, R.J. Young, and M. Halsall. Investigation into the deformation of carbon nanotubes and their composites through the use of Raman spectroscopy. *Composites: Part A*, 2001.

[30] M.M.J. Treacy, T.W. Ebbesen, and J.M. Gibson. Exceptionally high Young's modulus observed for individual carbon nanotubes. *Nature*, 381:678–690, 1996.

[31] A. Krishnan, E. Dujardin, T.W. Ebbesen, P.N. Yianilos, and M.M.J. Treacy. Youngs modulus of single-walled nanotubes. *Phys. Rev. B*, 58:14013–14019, 1998.

[32] F. J. Garca-Vidal, J. M. Pitarke, and J. B. Pendry. Effective medium theory of the optical properties of aligned carbon nanotubes. *Phys. Rev. Lett.*, 1997.

[33] Zu-Po Yang, Lijie Ci, James A. Bur, Shawn-Yu Lin, and Pulickel M. Ajayan. Experimental Observation of an Extremely Dark Material Made by a Low-Density Nanotube Array. *Phys. Rev. B*, 8:446–451, 2008.

[34] T. W. Ebbesen and P.M. Ajayan. *Nature*, 220:358, 1992.

[35] Yu-Chun Chen. PhD thesis, Auburn University, ECE Department, 2003.

[36] B.I. Yakobson and R.E. Smalley. *American Scientist*, 85:324, 1997.

[37] M.L. Terranova1, V. Sessa1, and M. Rossi. *Chemical Vapor Deposition*, 12:315–325, 2006.

[38] M. Daenen, R.D. de Fouw, B. Hamers, P.G.A. Janssen, K. Schouteden, and M.A.J. Veld. The Wondrous World of Carbon Nanotubes. 2003.

[39] M. Su, B. Zheng, and J. Liu. *Chem. Phys. Lett.*, 322:321, 2000.

[40] H. Lee, Y.S. Kang, P.S. Lee, and J. Y. Lee. *J. Alloys Compd.*, 330:569, 2005.

[41] P. Mauron, C. Emmenegger, A. Zuttel, C. Nutzenadel, P. Sudan, and L. Schlapbach. *Carbon*, 40:1339, 2002.

[42] J. B. Park, G. S. Choi, Y. S. Cho, S. Y. Hong, D. Kim, S. Y. Choi, J. H. Lee, and K. I. Cho. *J. Crystal Grwoth*, 244:211, 2002.

[43] M. Kumar and Y. Ando. *J. of Nanoscience and Nanotechnology*, 10:3739–3758, 2010.

[44] C. Adessi and M. Devel. *Phys. Rev. B*, 20, 2000.

[45] J.-M. Bonard, J.-P. Salvetat, T. Stockli, L. Forro, and A. Chatelain. *Appl. Phys. A.*, 69, 1999.

[46] Y. Satio and S. Uemura. *Carbon*, 2000.

[47] Yi-Chun Chen, Hsiu-Fung Cheng, Yun-Shuo Hsieh, and You-Ming Tsau. *J. Appl. Physic.*, 94, 2003.

[48] Goki Edal, Giovanni Fanchini1, and Manish Chhowalla1. *Nature Nanotechnology*, 2008.

[49] J.H. Hafner, C.-L. Cheung, A.T. Woolley, and C.M. Lieber. *Progress in Biophysics and Molecular Biology*, 77, 2001.

[50] Walt A. de Heer, Jean-Marc Bonard, Kai Fauth, Andr6 Chiitelain, Laszlo Forro, and Daniel Ugarte. *Advanced Materials*, 2004.

[51] Bishun N Khare, Patrick Wilhite, and M Meyyappan. *Nanotechnology*, 2004.

[52] Johannes Svensson, Niklas Lindahl, Hoyeol Yun, Miri Seo, Daniel Midtvedt, Yury Tarakanov, Niclas Lindvall, Oleg Nerushev, Jari Kinaret, SangWook Lee, and Eleanor E. B. Campbell. *Nano Letters*, 11:3569–3575, 2001.

[53] Chin-Lung Cheng, Chien-Wei Liu, Bau-Tong Dai, and Ming-Yen Lee. Physical and Electrical Characteristics of Carbon Nanotube Network Field-Effect Transistors Synthesized by Alcohol Catalytic Chemical Vapor Deposition. *J. of nanomaterials*, 2011, 2011.

[54] Y. Tzeng, C. Liu, and Z. Chen. Low temperature CVD carbon nanotubes on glass plates for flat panel display applications. In *Materials Research Society Spring Meeting*, 2000.

[55] Z.P. Huang, D.Z. Wang, J.G. Wen, M. Sennett, H. Gibson, and Z.F. Ren. Effect of nickel, iron and cobalt on growth of aligned carbon nanotubes. *Appl. Phys. A*, 2002.

[56] E. Flahaut, A. Govindaraj, A. Peigney, Ch. Laurent, A. Rousset, and C.N.R. Rao. Synthesis of single-walled carbon nanotubes using binary Fe, Co, Ni alloy nanoparticles prepared in situ by the reduction of oxide solid solutions. *Chemical Physics Letters*, 1999.

[57] Cheol Jin Lee, Jeunghee Park, and Jeong A. Yu. Catalyst effect on carbon nanotubes synthesized by thermal chemical vapor deposition. *Chemical Physics Letters*, 2002.

[58] Yoshikazu Homma, Yoshiro Kobayashi, Toshio Ogino, Daisuke Takagi, Roichi Ito, Yung Joon Jung, and Pulickel M. Ajayan. Role of Transition Metal Catalysts in Single-Walled Carbon Nanotube Growth in Chemical Vapor Deposition. *J. Phys. Chem. B*, 2003.

[59] M. Chhowalla, K. B. K. Teo, C. Ducati, N. L. Rupesinghe, G. A. J. Amaratunga, A. C. Ferrari, D. Roy, J. Robertson, and W. I. Milne. Growth process conditions of vertically aligned carbon nanotubes using plasma enhanced chemical vapor deposition. *J. of Applied Physics*, 2001.

[60] Chao Hsun Lin, Hui Lin Chang, Ming Her Tsai, and Cheng Tzu Kuo. Growth mechanism and properties of the large area well-aligned carbon nano-structures deposited by microwave plasma electron cyclotron resonance chemical vapor deposition. *Diamond and Related Materials*, pages 922–926, November 2002.

[61] R.H. Fowler and L.W. Nordheim. page 173, 1928.

[62] X. Lu, Q. Yang, C. Xiao, and A. Hirose. *Nonlinear Fowler-Nordheim plots of the field electron emission from graphitic nanocones: Influence of non-uniform field enhancement factor*. PhD thesis, 2006.

[63] C. Liu, Y.C., and Y. Tzeng. *Diamond and Related Materials*, 13:1274–1280, 2004.